INSTITUTE OF PHYSICS PUBLISHING REPORTS ON PROGRESS IN PHYSICS

Rep. Prog. Phys. **64** (2001) 97–146 www.iop.org/Journals/rp PII: S0034-4885(01)04040-4

Solar neutrinos

Michael F Altmann[1,3], Rudolf L Mößbauer[2] and Lothar J N Oberauer[2]

[1] Max-Planck-Institut für Physik (Werner-Heisenberg-Institut), 80805 München, Germany
[2] Technische Universität München, Physik Department E15, 85747 Garching, Germany

E-mail: altmann@mppmu.mpg.de

Received 9 November 2000

Abstract

Within the last decade solar neutrino physics has evolved into a field of relevance not only for probing our understanding of stellar physics, but also for investigating and pinpointing intrinsic neutrino properties, most importantly neutrino masses and mixing angles. To date, results from six different and partly complementary experiments have been acquired. Taken together, these experimental data provide evidence for neutrino oscillations, i.e. neutrino masses and mixing, and thus physics beyond the standard model of electroweak interactions. Several new experiments currently being planned or constructed will commence operation within the next few years. They will provide additional complementary data and allow—together with the already running detectors—performance of a full solar neutrino spectroscopy in both the charged-current and the neutral-current detection mode. Performing a thorough comparison of the spectral shape observed on Earth and the neutrino spectrum expected from solar model computations will be essential for further pinpointing neutrino masses and mixing parameters. This article, after giving a short introduction to the field, reviews the current status of solar neutrino physics and gives an outlook on the potential which the upcoming experiments offer for further progress.

[3] Author to whom any correspondence should be addressed.

0034-4885/01/010097+50$90.00

Contents

1. Solar neutrino physics: history

Neutrinos, being neutral particles, are subject only to the weak interaction (and gravity). Therefore their detection in terrestrial detectors of at most a few hundred tons of material becomes very difficult.

Neutrinos were first introduced into physics as hypothetical particles by Wolfgang Pauli in 1930; see [114]. Pauli had to cope at that time with the fact that electrons emitted in ordinary radioactive decays exhibited a continuous spectrum, suggesting the introduction of a three-body rather than a two-body decay. His theory had been formulated, however, before the discovery of the neutron. A two-particle decay led to a statistics which was not in agreement with the results of optical spectroscopy, while a three-particle decay could explain the continuous form of the electron spectrum and yielded the right statistics, but gave rise to a series of other problems, which were only solved in 1932 with the discovery of the neutron by Chadwick [36]. The third particle, which had been introduced by Pauli to add to the proton and electron, was finally called the neutrino by Fermi, meaning 'little neutron' in Italian. Though the existence of the neutrino had been seen earlier in recoil experiments [122], it remained for Fred Reines *et al* [41, 121], in about 1956, to discover the neutrino in an actual reaction. This reaction, which even nowadays is still used in antineutrino observations, reads in modern language $\mathrm{p} + \bar{\nu}_\mathrm{e} \rightarrow \mathrm{n} + \mathrm{e}^+$. This first discovery of the neutrino won Reines the Nobel Prize in 1995.

While complete parity conservation would require neutrinos to be of both helicities, complete parity violation would involve only one helicity, as has been observed experimentally by Goldhaber *et al* [74], according to whom neutrinos are emitted with only left-handed helicity, ν_L. This follows nowadays also from the standard theory $\mathrm{SU}(2)_L$ of electroweak interactions. This theory assumes that only ν_L and $\bar{\nu}_R$ feel the weak forces. Thus, only the left-handed fermions form doublets:

$$\begin{array}{lll} (\mathrm{u}, \mathrm{d}')_L & (\mathrm{c}, \mathrm{s}')_L & (\mathrm{t}, \mathrm{b}')_L \\ (\nu_\mathrm{e}, \mathrm{e}^-)_L & (\nu_\mu, \mu^-)_L & (\nu_\tau, \tau^-)_L \end{array}$$

where the use of primes indicates that we are referring to the weak eigenstates of the down, strange, and beauty quarks, which result from the mass eigenstates (d, s, b) via a unitary transformation. The right-handed fermions, which do not participate in the weak interactions, are singlets. We shall use the notation for chirality $\nu_L = (1 + \gamma_5)\nu$ and $\bar{\nu}_R = (1 + \gamma_5)\bar{\nu}$, where $\gamma_5 = \prod_{i=0}^{3} \gamma_i$.

Lederman, Schwartz, and Steinberger discovered in 1962 the existence of a second type of neutrino [47]. Today we know that there are only three types of light neutrino. This knowledge arises from experiments at CERN [32, 33], which measured the total width of the Z^0 resonance, attributing widths to six quarks, three charged leptons, and three light neutral leptons, assuming the latter to have equal width. This procedure does not exclude heavier neutrinos with $m_\nu \gtrsim 45$ GeV. The three types of light neutrino are called ν_e (electron neutrino), ν_μ (muon neutrino), and ν_τ (tau neutrino).

While we know a lot about the quarks and the charged leptons, we still know very little about the neutrinos, including their mass values. Direct measurements of neutrino masses due to their extremely small values yield at present only limits: $m(\nu_\mathrm{e}) < 2.2$ eV (95% c.l.) [144], $m(\nu_\mu) < 0.16$ MeV (90% c.l.) [12], $m(\nu_\tau) < 18.2$ MeV (95% c.l.) [33].

There also exists a theoretical mass limit for neutrinos of cosmological origin: attributing the entire mass of the Universe to neutrinos only, and adding for safety reasons a factor of two to the critical mass of the Universe, we arrive at a theoretical mass limit, which is given by $\sum_{i=1}^{3} m(\nu_i) \lesssim 10^2$ eV.

Information on the masses of neutrinos is available from three types of experiment:

(a) Direct determination of masses from kinematical experiments (energy and momentum balance).
(b) Neutrinoless double β-decay (0ν–$\beta\beta$ decay).
(c) Neutrino oscillations.

As will be elucidated in the following section, neutrino oscillations in particular, being a quantum mechanical interference effect, open the prospect of detecting even tiny mass differences between neutrino eigenstates. Using electron neutrinos emitted by the Sun, neutrino masses down to $m_\nu \lesssim 10^{-6}$ eV can be investigated.

2. Neutrino oscillations

2.1. Neutrino masses and mixing

Neutrino oscillations are oscillating transitions $\nu_\alpha \leftrightarrow \nu_\beta$ ($\alpha, \beta = \mathrm{e}, \mu, \tau$), where one kind of neutrino transfers into another kind of neutrino distinguished by different leptonic quantum numbers. We are usually dealing with 'flavour' oscillations, where the total lepton number is conserved, $\Delta L = 0$, and only conservation of the family lepton numbers L_α is violated. The idea of neutrino oscillations of the type particle $\leftrightarrow$ antiparticle ($\nu \leftrightarrow \bar{\nu}$) was first introduced in 1958 by Pontecorvo [115], i.e. long before the observation of the second type of neutrino. The idea of the mixing of massive neutrinos was introduced in 1962 by Maki [110]. Two-flavour oscillations were also discussed by Pontecorvo in 1967 [116, 117]. A consistent phenomenological theory of neutrino mixing and oscillations was developed in 1969 by Gribov and Pontecorvo [79]. In the case of quarks, such mixing and the associated oscillations are well known. Here it is observed, though theoretically not understood, that the eigenstates (d′, s′, b′) entering the weak charged current are orthonormal linear combinations of the energy eigenstates (d, s, b) of quarks. The weak eigenstates are thereby those states which are produced in weak decays, while the energy eigenstates are those states which determine the propagation of particles in the vacuum, i.e.

$$|\nu(t, x)\rangle = |\nu(0)\rangle \exp(-\mathrm{i}(Et - \vec{p} \cdot \vec{x})).$$

The relation between the two kinds of eigenstate is given by the Cabibbo–Kobayashi–Maskawa mixing matrix:

$$\begin{pmatrix} \mathrm{d}' \\ \mathrm{s}' \\ \mathrm{b}' \end{pmatrix} = \begin{pmatrix} U_{\mathrm{d}1} & U_{\mathrm{d}2} & U_{\mathrm{d}3} \\ U_{\mathrm{s}1} & U_{\mathrm{s}2} & U_{\mathrm{s}3} \\ U_{\mathrm{b}1} & U_{\mathrm{b}2} & U_{\mathrm{b}3} \end{pmatrix} \begin{pmatrix} \mathrm{d} \\ \mathrm{s} \\ \mathrm{b} \end{pmatrix}.$$

This connection is linear as a consequence of basic principles of quantum mechanics. Due to redundancies, it is sufficient to write this relation between either the upper or lower states of the quark families, where for quarks the lower states have been chosen. The nine complex coefficients of the mixing matrix reduce to nine real coefficients because of the unitarity condition. Again because of redundancies, these are reduced further to four parameters, three being mixing angles and one being a phase. There appears no physical reason that such a connection should not exist also for leptons. Again because of redundancies, one might write such a relation for either the upper or lower states of the leptons, where it is customary to use the upper states, i.e. the neutrinos, in order to leave the mass determinations of the charged

leptons unchanged. Like in the case of quarks, there are only four relevant parameters in the mixing matrix.

Two conditions are necessary for the appearance of neutrino oscillations:

(1) Lepton family quantum numbers are not strictly conserved, $\Delta L_\alpha \neq 0$.
(2) At least two neutrinos differ in their mass values. If all neutrino masses are equal (i.e. complete degeneracy, $m_i = m$), then $\langle \nu_\beta | M | \nu_\alpha \rangle = m\delta_{\alpha\beta}$ because of unitarity. Oscillatory transitions $\nu_\alpha \leftrightarrow \nu_\beta$ would then be impossible.

Because neutrino oscillations exist only if neutrino masses exist, there is apparently a close connection between neutrino oscillations and neutrino masses. The question arises here of why neutrinos should have any mass value at all. Neutrinoless $\beta\beta$-processes, which would imply a lower bound on neutrino mass, have not yet been observed. This fact does not, however, imply an upper bound on the mass of the neutrinos, because the matrix elements may exhibit cancellations. Neutrinos appear in weak interactions only with definite chirality. Massive neutrinos, on the other hand, require both chiralities, which would require a deviation from the present standard model. Such a deviation, nevertheless, is possible. Massive neutrinos might also partially be candidates for the missing dark matter in the Universe. They furthermore might settle the question of whether the Universe is open, closed or flat. The rest mass of the photon is zero, which is a consequence of the gauge invariance of the electromagnetic interaction. For neutrinos, however, there is no similar invariance principle known. It furthermore has to be explained why neutrino masses (if they exist) are much smaller than the masses of charged leptons. The seesaw principle offers a remedy, yet at the expense of the introduction of Majorana neutrinos.

2.2. Neutrino oscillations in vacuum

There are two types of experiment which might be envisaged:

(1) Appearance experiments, where one searches for the appearance of states with a new flavour in a beam. Such experiments are by necessity particularly sensitive to mixing parameters.
(2) Disappearance experiments, where one looks for the disappearance of neutrinos of the initial flavour from a beam. Such experiments might involve, in particular, electron neutrinos, in case there is not sufficient energy available to create neutrinos of another kind. Such is the situation with reactor-produced neutrinos and solar neutrinos, whose energy is far below the rest masses of the charged μ- and τ-leptons. These kinds of experiment are particularly sensitive to small energies and therefore also to small mass values.

For solar neutrinos, only the experimental situation (2) is feasible for energetic reasons. In the scheme with neutrino mixing, the neutrino flavour states are coherent superpositions of the state vectors of neutrinos with different masses. This is the basic quantum mechanical reason for the phenomenon of oscillations. We shall therefore discuss the problem of coherence: non-degenerate mass eigenstates propagate with different velocities and must therefore have been emitted at different times or places if they arrive on Earth at the same time or in the same place. Interference between different mass eigenstates will only occur if the source remains coherent over a time interval comparable to the difference in arrival times. The quantum mechanical condition for such an interference is $(v_1 - v_2)t \leqslant c\tau_{\mathrm{coh}}$. Here, t is the transit time of photons for the distance d between the Sun and the Earth, $t \approx d/c$, while v_i is the transit velocity of the ith massive component between the Sun and the Earth and τ_{coh} is the coherence time within the Sun, which is essentially given by the collision time for one proton with another. The times involved differ somewhat according to author: we have Nussinov

et al [113], who arrives for mere proton–proton collisions at values $\tau_{\rm coh} = 10^{-17}$ s, Kraus and Wilczek [99], who arrive at $\tau_{\rm coh} = 10^{-15}$ s, taking into account that we are really dealing with a plasma, where collisions between protons and electrons matter, and Loeb [108], who arrives at 5×10^{-15} s, by writing down all effects and coming to the conclusion that proton–proton collisions dominate. In any case, we obtain in all theories for the vacuum oscillations in the Sun–Earth distance full coherence for the ^{8}B neutrinos and even more so for all neutrinos of lower energy. For the energies within the Sun where we might have the MSW effect to be described below; full coherence is even more definitely present. It should be noted that the problem of coherence was also treated by Stodolsky [132], who came to the conclusion that the energy spectrum already contains all pertinent information.

If neutrinos appear in a mixed state, then we may have neutrino decay. The absence of γ-rays from SN1987A shows, however, that the lifetimes of solar neutrinos are sufficiently long to consider them to be constant. Neutrino oscillations like quark oscillations have the prerequisite that eigenstates of the energy (or mass, in the case where the momentum of a neutrino beam can be considered constant) and weak-interaction eigenstates differ, i.e. that their relation has non-diagonal matrix elements. We shall discuss such oscillations now in the presence of three neutrino states $\nu_{\rm e}$, ν_μ, ν_τ. The connection is (for quantum mechanical reasons) given by a unitary transformation U, which is also called the mixing matrix:

$$|\nu_\alpha\rangle = \sum_i U_{\alpha i} |\nu_i\rangle$$

and the inverse

$$|\nu_i\rangle = \sum_\alpha (U^\dagger)_{i\alpha} |\nu_\alpha\rangle = \sum_\alpha U^\star_{\alpha i} |\nu_\alpha\rangle$$

where $U^\dagger U = 1$.

We shall in the following assume neutrino masses to all have the same momentum state, i.e. we shall assume the neutrino beams to have a common momentum. Being eigenstates of the mass matrix, the states are stationary states, i.e. they have a time dependence[4]

$$\nu_i(t) = \exp(-{\rm i}E_i t)\nu_i(t=0)$$

where

$$E_i = \sqrt{p_\nu^2 + m_i^2} \approx p_\nu + m_i^2/(2p_\nu) \approx E_\nu + m_i^2/(2E_\nu)$$

and we have assumed $p_\nu \gg m_i$, i.e. highly relativistic neutrinos. A pure flavour beam $\nu_\alpha(0) = \nu_\alpha$ at time zero thus would develop over time into the beam

$$\nu(t) = \sum_i U_{\alpha i} \exp(-{\rm i}E_i t)\nu_i = \sum_{i,\beta} U_{\alpha i} U^\star_{\beta i} \exp(-{\rm i}E_i t)\nu_\beta .$$

One usually measures probabilities. The probability of finding ν_β at $L \approx t$ for light (i.e. relativistic) neutrinos is given by

$$P(\nu_\alpha \to \nu_\beta) = \left| \sum_i U_{\alpha i} U^\dagger_{i\beta} \exp\left(-{\rm i}\frac{m_i^2}{2p_\nu}t\right)\right|^2 \tag{1}$$

$$= \sum_i |U_{\alpha i} U^2_{i\beta}|^2 + {\rm Re} \sum_i \sum_{j\neq i} U_{\alpha i} U^\dagger_{i\beta} U_{\alpha j} U^\dagger_{j\beta} \exp\left({\rm i}\frac{\Delta m^2_{ij} L}{2E_\nu}\right) \tag{2}$$

where $\Delta m^2_{ij} = |m_i^2 - m_j^2|$.

[4] For simplicity, we omit in the following the brackets $|\,\rangle$ denoting neutrino states.

A straightforward calculation yields in the two-neutrino approximation for the probabilities P of observing a neutrino of type ν_β, if one has started at the origin with neutrino type ν_α,

$$P(\nu_\alpha \to \nu_\beta) = P(\bar{\nu}_\alpha \to \bar{\nu}_\beta) = \frac{1}{2}\sin^2 2\theta\left(1 - \cos\frac{\Delta m^2 t}{2E_\nu}\right) \tag{3}$$

$$= \sin^2 2\theta \sin^2\left(1.27\frac{(\Delta m^2/\mathrm{eV}^2)(L/\mathrm{m})}{(E_\nu/\mathrm{MeV})}\right) \tag{4}$$

if practical units are used and $\alpha \neq \beta$.

This relation clearly shows the oscillatory behaviour of the neutrino oscillations, where one starts with one kind of neutrino and generates either new types of neutrino ($\alpha \neq \beta$) or simple deviations of the neutrinos from ordinary expectations ($\alpha = \beta$). It should be noted in this context that in the oscillatory probability, smaller values of Δm^2 require larger values of the distance L. The expression for neutrino oscillations yields the normalized transition probability for neutrino oscillations:

$$P(\nu_\mathrm{e}(0) \to \nu_\mu(t)) = \sin^2 2\theta(1 - \cos(E_2 - E_1))$$

which clearly shows the appearance of an interference term containing the phase

$$\phi = (E_2 - E_1)t = (\Delta m^2/2p_\nu)t.$$

From such experiments one therefore can get information on the mass parameter Δm^2, whereas from experiments, where either probabilities of decay processes or reaction cross-sections are measured, one only gets information on the squares of matrix elements of the weak interaction.

The direct observation of neutrino oscillations has been announced numerous times, but so far always prematurely, with the possible exception of the observation of atmospheric neutrinos in SUPERKAMIOKANDE, which might be genuine and if so would give rise to neutrino masses. Another announcement of neutrino oscillations was recently made by a Los Alamos group [14]. State mixing does not occur with neutrinos generated by a neutral-current interaction. Neutral-current interactions are in first order, in fact, diagonal in quark and lepton fields, a consequence of the Glashow–Iliopoulos–Maiani (GIM) [149] mechanism (or more generally the Cabibbo–Kobayashi–Maskawa mechanism). The mechanism provides for the vanishing of neutral currents with family mixing. By consequence, neutral-current interactions produce no flavour changes and no neutrino oscillations. There arises an immediate application to the Sun: a measurement of solar neutrinos by neutral-current interactions as envisaged by SNO, SUPERKAMIOKANDE and BOREXINO would provide the entire neutrino flux from the Sun irrespective of oscillations between the three flavours and might therefore serve as a calibration of neutrinos from the Sun—with the possible exception of neutrino oscillations to a hypothetical 'sterile' neutrino that does not couple with the weak neutral current.

2.3. Matter-enhanced oscillations

The MSW (Mikheyev, Smirnov, Wolfenstein) effect in matter was first discovered by Wolfenstein [147, 148] and later on applied to a resonance effect by Mikheyev and Smirnov [111]. The probability for flavour transitions can thereby be drastically increased, even if in vacuum only small probabilities prevail. This holds, in particular, for the Sun. If neutrinos are propagating in matter, we experience the interaction of the neutrinos with the electrons in matter. This results in an additional contribution in the Hamiltonian, and we obtain for a two-neutrino approximation after diagonalization

$$H_m = \frac{1}{2p}\begin{pmatrix} m_{2m}^2 & 0 \\ 0 & m_{1m}^2 \end{pmatrix}$$

with the eigenstates in matter:

$$m^2_{1m,2m} = \frac{1}{2}\left[m_1^2 + m_2^2 + A \mp \sqrt{(A - D\cos 2\theta)^2 + D^2 \sin^2 2\theta}\right] \tag{5}$$

where $D = \Delta m^2 = m_2^2 - m_1^2$ and $A = 2\sqrt{2}G_F N_e p$. G_F is the Fermi constant and N_e the local electron density. For the mass-squared splitting of the matter eigenstates, we obtain

$$\Delta m^2_m := m^2_{2m} - m^2_{1m} = D\sqrt{(A/D - \cos 2\theta)^2 + \sin^2 2\theta}.$$

Rewriting the Hamiltonian in the $(\nu_e, \nu_\mu)^T$ basis of the flavour eigenstates, we obtain (non-diagonal representation)

$$H^\alpha_m = \frac{1}{2p}\begin{pmatrix} m^2_{ee} + A & m^2_{e\mu} \\ m^2_{e\mu} & m^2_{\mu\mu} \end{pmatrix} = \frac{1}{4p}\begin{pmatrix} m_1^2 + m_2^2 - D\cos 2\theta + 2A & D\sin 2\theta \\ D\sin 2\theta & m_1^2 + m_2^2 + D\cos 2\theta \end{pmatrix}.$$

Here, the non-diagonal character of the interaction with the electrons should be noted—an interaction which does not exist with the other types of charged lepton. The reason is that the ν_e interact with the electrons in the solar matter via both $W^\pm$ and Z^0 exchange, whereas the ν_μ and ν_τ are subject to only the neutral-current interaction. Electron neutrinos, therefore, 'feel' an additional potential when traversing matter. The mixing matrix in matter, U_m, with the mixing angle in matter, θ_m, is defined by

$$\begin{pmatrix} \nu_e \\ \nu_\mu \end{pmatrix} = \begin{pmatrix} \cos\theta_m & \sin\theta_m \\ -\sin\theta_m & \cos\theta_m \end{pmatrix}\begin{pmatrix} \nu_{1m} \\ \nu_{2m} \end{pmatrix}$$

and its inverse

$$\begin{pmatrix} \nu_{1m} \\ \nu_{2m} \end{pmatrix} = \begin{pmatrix} \cos\theta_m & -\sin\theta_m \\ \sin\theta_m & \cos\theta_m \end{pmatrix}\begin{pmatrix} \nu_e \\ \nu_\mu \end{pmatrix}$$

with the mixing angle given by $\tan 2\theta_m = \sin 2\theta/(\cos 2\theta - A/D)$, where

$$\sin 2\theta_m = \frac{\sin 2\theta}{\sqrt{(A/D - \cos 2\theta)^2 + \sin^2 2\theta}}.$$

In passing, we note that for vanishing electron density $N_e \to 0$, i.e. $A \to 0$, we naturally have $m^2_{1m,2m} \to m^2_{1,2}$, $D_m \to D$, and $\theta_m \to \theta$.

For the case of a resonance in matter ($A/D \approx \cos 2\theta$), we have $A = A^{\mathrm{Res}} = D^{\mathrm{Res}} \cos 2\theta$, and we obtain for the amplitude of the oscillation the maximum value $\sin^2 2\theta^{\mathrm{Res}}_m = 1$, or $\theta^{\mathrm{Res}}_m = \pi/4$. Because

$$\sin^2 2\theta_m = \frac{\sin^2 2\theta}{([A/p_\nu]/[D/p_\nu] - \cos 2\theta)^2 + \sin^2 2\theta} \propto \frac{1}{(E - E_0)^2 + (\Gamma_{\mathrm{FWHM}}/2)^2} \tag{6}$$

represents a Breit–Wigner distribution, we have a total width of the resonance, which is given by $\Gamma_{\mathrm{FWHM}} = 2(D/p_\nu)\sin 2\theta$, thus growing with the vacuum mixing angle θ according to $\sin 2\theta$.

It should be noted that antineutrinos would not lead to a resonance phenomenon. This is a consequence of the fact that the sign of an interaction does not matter, as long as the interaction appears as a single one, while this sign matters when two types of interaction matter, as is the case with neutrinos in matter. Wolfenstein in his first publication [147] had indeed chosen the wrong sign for the weak interaction, which later on was corrected by Langacker [103].

It should also be noted that (neglecting neutral-current weak interaction which is the same for all neutrino flavours) the eigenvalue m_1 of ν_μ is not influenced, while the eigenvalue m_2 of ν_e grows in proportion to N_e. This situation is reflected by the dashed lines in figure 1. In

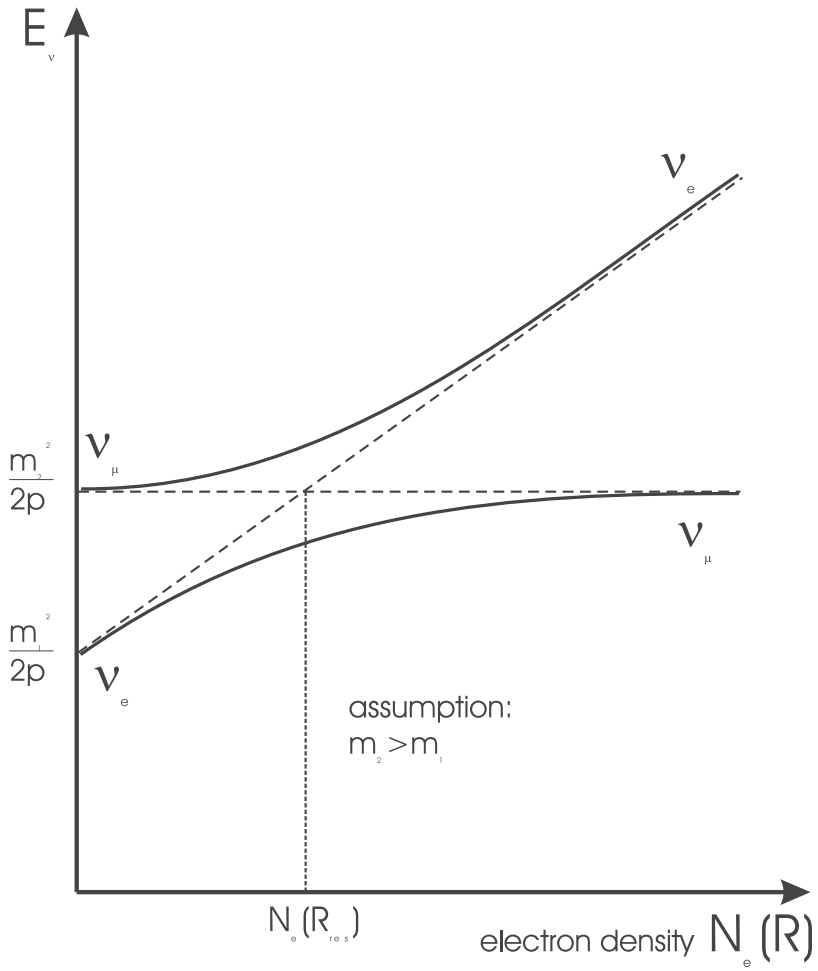

Figure 1. The MSW effect in the two-neutrino approximation, assuming $m_2 > m_1$. The neutral-current (nc) interaction common to all neutrinos has been suppressed. The ν_e are produced in the solar centre. In the non-interaction scheme their interaction is proportional to the solar electron density, which leads to the descent shown in the plot. Any ν_μ present stay constant, because they are not influenced by the electrons in the Sun. In the case of an interaction, the curve is followed, with the ν_e being created in the solar centre and the ν_μ leaving the solar surface. Because the process depends on energy, only a certain fraction of the ν_μ are leaving the Sun. If the upper curve is followed, we speak of adiabatic transitions. Non-adiabatic transitions lead to transitions between the curves (straight line).

the presence of neutral currents, the curves shown in figure 1 will hold. In the presence of adiabaticity, the neutrinos will follow only one curve, while the absence of adiabaticity will induce transitions between the curves.

Neutrinos involved in the MSW effect are generated in the solar centre as electron neutrinos. Above a certain energy, these neutrinos convert into muon neutrinos, which leave the Sun and are not registered by any terrestrial detector, which is only sensitive to electron neutrinos—as are e.g. the radiochemical experiments. Because only neutrinos above a certain energy are influenced by the MSW effect, only a certain fraction of all neutrinos will participate in the MSW effect. Similar remarks also hold for the question of adiabaticity.

3. Solar neutrino production

Starting in 1920 when Eddington proposed a nuclear origin for the tremendous energy radiated by stars [51], increasingly detailed models and numerical computations describing the stellar structure, dynamics, and evolution have been constructed and confronted with measurements. The Sun, a main-sequence star in the middle of its hydrogen-burning stage, has played a prominent role in the gaining of insight into the physics of stars, as it is close enough to allow us to experimentally probe many predictions of the model computations. This relates not only to observation of the surface, but also to that of the solar interior by means of neutrinos and seismic waves.

In the following we will first describe the basic ideas underlying the reference solar model[5]. We will then focus on the thermonuclear processes taking place in the solar core, and discuss the neutrino fluxes and spectra emerging from them. Finally, the accuracy of these predictions will be investigated. In this context, it is instructive to confront the reference solar models with helioseismological measurements. Within the last few years these observations have allowed possible physical scenarios to be constrained and have served to put the reference solar model on a stable basis, whereas most non-standard solar models proposed *ad hoc* to escape the observed solar neutrino flux deficit have been disproved.

3.1. Basic ideas of the solar model

Modelling the solar interior requires us not only to describe the present solar structure, but also to explain the evolution of the Sun from the initial ignition of hydrogen nuclear fusion to the present day. The reference solar models (see e.g. [19, 30]) are based on a set of plausible assumptions:

- Solar energy generation is due to thermonuclear fusion of hydrogen to helium. The energy release is 26.73 MeV per ^{4}He nucleus produced.
- The sun is in hydrostatic equilibrium. This means that the hydrostatic pressure resulting from thermonuclear fusion must exactly counterbalance gravity. One further assumes thermal equilibrium, i.e. that the energy produced by nuclear reactions balances the total energy loss, which is the sum of the radiative energy flux $L_\odot$ and the energy carried away by neutrinos.
- Energy transport from the solar centre where nuclear fusion takes place ($r \lesssim 0.2\ R_\odot$) outwards to the surface occurs, apart from the neutrinos, by electromagnetic radiation and convection. The latter is particularly important for the outer region $r > 0.7\ R_\odot$, the so-called convection zone, whereas in the central part of the Sun, radiative transport is the most efficient process (radiative zone)[6]. In the dense matter of the solar plasma, photons interact with electrons, atoms, ions, and molecules. These interactions are summarized in the so-called 'Rosseland mean opacities' $\kappa(T, \rho, \text{composition})$, which govern the radiative energy transport and thus the temperature profile inside the Sun.
- Initially, the composition elements of the Sun were distributed homogeneously. Since then, changes of element abundances have occurred only as a result of nuclear fusion reactions.

[5] Following [137], by the term *reference model* we mean a state-of-the-art solar model which incorporates all physical processes considered relevant for the Sun, using the best available input parameters. In contrast to popular practice, we avoid speaking of a 'standard solar model', in order to stress that the quantitative results of such a model computation are time dependent in the sense that refined input numbers and improved descriptions of the physical processes are continuously being included.

[6] Conductivity, which is important for high-density stars, plays no role for the Sun.

An equation of state for the solar interior (see e.g. [123]) describes the relation between pressure $p(r)$, density $\rho(r)$, temperature $T(r)$, energy generation per mass unit $\varepsilon(r)$, luminosity $L(r)$, and opacity $\kappa(r)$, where r is the radial distance from the solar centre. Obviously, the equation of state will depend on the mass fractions of hydrogen, X, helium, Y, and 'heavy' (i.e. heavier than helium) elements, Z (so-called 'metals'). Element diffusion is generally taken into account in more recent models.

A number of measured quantities enter into and constrain the solar models. Among them are radiative opacities which have to be calculated for the conditions inside the Sun and are available in tabulated form [101], nuclear fusion cross-sections (see section 2.1), the solar radius $R_\odot$ and surface temperature $T_\odot$, the surface luminosity $L_\odot$, and the solar mass and age.

Utilizing the basic assumptions and measured input data and incorporating the physical processes considered relevant for the solar interior (e.g. diffusion and screening enhancement of nuclear reactions), a self-consistent numerical computation of the solar structure and evolution is performed. It yields, among other things, predictions for the solar core temperature T_c, the rates at which the various nuclear fusion reactions contribute to the ^{4}He generation (cf. section 2.2), whence the neutrino fluxes for the individual branches, the depth of the radiative zone, and the temperature and density profile inside the Sun.

In table 1 we list some relevant physical data for the Sun, and, in addition, predictions of two reference solar models.

Within recent years, accurate measurements of solar seismic modes (pressure (p-) modes) (see e.g. [75, 76, 85]) have allowed independent inference of the speed of sound $c_s(r)$ (and therefrom via $c_s \propto \sqrt{(T/\rho_M)}$ (with ρ_M being the mean molecular weight) the solar density profile) inwards to about 0.05 $R_\odot$ [19,37] and, in addition, the boundary radius of the convective zone, R_{CZ}. This quantity can be determined from helioseismological measurements, since for $r < R_{\mathrm{CZ}}$ the temperature gradient is determined by the requirement of radiative energy transport, whereas in the convective zone the gradient is nearly adiabatic due to the highly effective convective transport. From this sharp boundary a pronounced transition in $\mathrm{d}T/\mathrm{d}r$ and, accordingly, in $\mathrm{d}c_s^2/\mathrm{d}r$ occurs, which allows precise location of R_{CZ}. Confronting the results from helioseismology with the respective solar model predictions for $c_s^2(r)$ showed an intriguing agreement, better than 0.01 for the relative uncertainty (Sun model)/Sun [17,19,127]. This result supports the reference solar model as a reliable description of the Sun and strongly disfavours most non-standard solar models (cf. e.g. [140]).

3.2. Thermonuclear processes: pp and CNO cycles

The Sun liberates its energy in nuclear fusion reactions taking place in the solar core at radii $r \lesssim 0.25\ R_\odot$, where hydrogen is burnt to ^{4}He. This takes place in a network of (essentially) two-particle nuclear reactions, the pp cycle shown in figure 2 being most important for the temperature domain characterizing the solar core.

Several of the reactions result in the emission of electron neutrinos ν_{e} of characteristic energy and spectral shape, as can be seen from figure 2(b). For the calculation of neutrino flux predictions, knowledge of the branching ratios for the alternative subchains is essential. The reaction rate per unit volume, $\dot{n}_{\mathrm{ab}}$, for a two-particle nuclear reaction is given by

$$\dot{n}_{\mathrm{ab}} = n_{\mathrm{a}} n_{\mathrm{b}} \int v\sigma(v) f(v)\, \mathrm{d}v = n_{\mathrm{a}} n_{\mathrm{b}} \langle \sigma v \rangle$$

with n_{a} and n_{b} being the particle number densities, v the particle velocity, $\sigma(v)$ the reaction cross-section, and $f(v)$ the Maxwellian velocity distribution, where we have implicitly assumed local thermodynamic equilibrium.

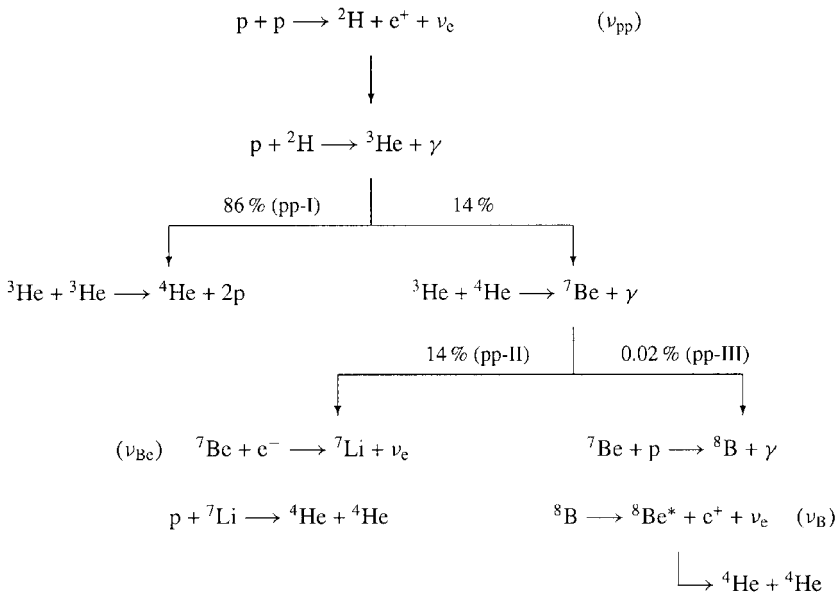

(a)

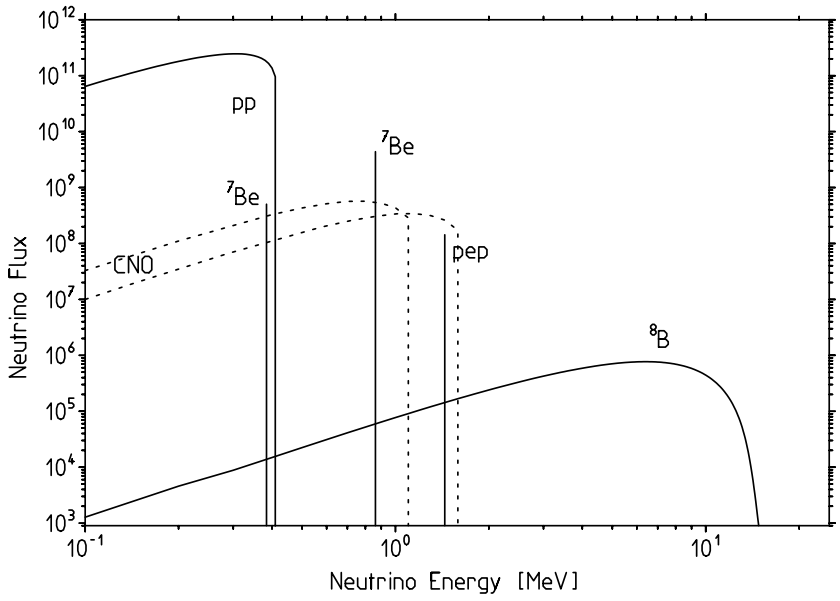

(b)

Figure 2. The pp cycle is the dominant energy generation mechanism in the Sun. It is subdivided into four chains, the pp-I chain being by far the most frequent cycle termination (86% pp-I, 14% pp-II, <0.1% pp-III, $\lesssim 10^{-3}$% pp-IV). The pp-IV reaction $^3\mathrm{He} + \mathrm{p} \rightarrow {}^4\mathrm{He} + \nu + \mathrm{e}^+$, giving rise to the continuous spectrum of so-called hep neutrinos, is omitted in the figure. Panel (b) shows the neutrino spectrum resulting from the solar fusion reactions. Solid lines correspond to neutrinos from the pp cycle, dotted lines to those from the CNO cycle, which, however, plays only a minor role for the Sun. Fluxes are given in units of $\mathrm{MeV}^{-1}\ \mathrm{cm}^{-2}\ \mathrm{s}^{-1}$ for continuous spectra and $\mathrm{cm}^{-2}\ \mathrm{s}^{-1}$ for lines.

Table 1. Physical data and characteristics of the Sun. The upper group lists measured values acting as constraints for the reference solar models, whereas the lower group shows predictions from two prominent reference models, from [19] (BBP98) and [30] (BTM98). The individual neutrino fluxes will be dealt with in detail in section 3.2.

Mass	$(1.989 \pm 0.001) \times 10^{30}$ kg	
Radius	$(6.960 \pm 0.001) \times 10^{8}$ m	
Age	$(4.52 \pm 0.04) \times 10^{9}$ a [30]	
Surface luminosity $L_\odot$	$(3.845 \pm 0.008) \times 10^{26}$ W	
Surface temperature	5.78×10^{3} K	
Present He mass fraction (surface) Y	0.249 ± 0.003 [26]	
Metal mass fraction Z/X	0.0245 [131]	
Boundary of convective zone R_{CZ}	$(0.713 \pm 0.001)\ R_\odot$ [25]	
	BBP98 [19]	BTM98 [30]
Core temperature T_c		15.67×10^{6} K
Contribution of pp cycle to E-generation	98.3%	98.74%
Contribution of CNO cycle to E-generation	1.7%	1.26%
Individual solar neutrino fluxes at $r = 1$ AU (in 10^7 cm^{-2} s^{-1})):		
pp flux	$5.94 \times 10^{3} \times (1.00 \pm 0.01)$	5.99×10^{3}
pep flux	$13.9 \times (1.00 \pm 0.01)$	14.1
Be flux	$480 \times (1.00 \pm 0.09)$	470
B flux	$5.15 \times 10^{-1} \times (1.00^{+0.19}_{-0.14})$	4.82×10^{-1}
hep flux	2.1×10^{-4}	
N flux	$60.5 \times (1.00^{+0.19}_{-0.13})$	46.7
O flux	$53.2 \times (1.00^{+0.22}_{-0.15})$	46.7
F flux	$6.33 \times 10^{-1} \times (1.00^{+0.12}_{-0.11})$	

At the solar core temperature the average thermal particle energy is several keV only, substantially smaller than the repulsive Coulomb barriers which are in the MeV range. The number of particles in the high-energy tail of the Maxwellian distribution being much too small for 'classical' reactions to occur at a non-negligible rate, the relevant process is barrier penetration via the tunnelling effect [69]. As the probability for quantum mechanical s-wave tunnelling in the WKB approximation exhibits an exponential energy dependence, the reaction rate at low energy can be written as

$$\dot{n}_{ab} = n_a n_b \left(\frac{8}{m\pi}\right)^{1/2} (kT)^{-3/2} \int_0^\infty S(E) \exp\left(-\frac{E}{kT} - \frac{2\pi Z_a Z_b e^2 \sqrt{m}}{h\sqrt{2E}}\right) \mathrm{d}E \tag{7}$$

where Z are the nuclear charges, m the reduced mass, and $S(E)$ denotes the so-called astrophysical S-factor:

$$S(E) := \sigma(E) E \exp(2\pi Z_a Z_b e^2 \sqrt{m}/(\hbar\sqrt{2E}))$$

which, in contrast to $\sigma(E)$, exhibits (except for resonances) only a smooth variation with energy.

The convolution of the exponentially decreasing Maxwell–Boltzmann distribution and the quantum mechanical penetration factor increasing with energy results in an overlap region

where the reaction probability is non-negligible. This energy region, being typically in the range of ≈10– 50 keV for the reactions of the solar pp chain, is called the 'Gamow peak'. For characterizing reaction rates and experimental cross-section measurements, the astrophysical S-factor and its derivatives $S' = \mathrm{d}S/\mathrm{d}E$, $S'' = \mathrm{d}^2S/\mathrm{d}E^2$ are usually quoted at zero energy, rather than for the energy of the Gamow peak, E_0. To associate $S(0)$ with the above formula, an approximative expansion is applied [5, 15, 137].

In laboratory measurements all pp-cycle reactions except (due to the tiny cross-sections) (i) the initiating one, p(p, νe^+)^{2}H, and (ii) the hep reaction, ^{3}He(p, νe^+)^{4}He, can be investigated. However, the steep decrease of the reaction rates at low energy makes measurements in the regions of the Gamow peaks extremely difficult. Therefore, except for a recent determination of S_{33}, characterizing the reaction ^{3}He(^{3}He, 2p)^{4}He, which was performed with a dedicated accelerator under low-background conditions in the Gran Sasso Underground Laboratory [29, 93, 94, 109], extrapolations of measurements done at higher energies of order 100 keV to several MeV have to be utilized. In passing, we note that special care has to be exercised for certain reactions, e.g. ^{7}Be(p, γ)^{8}B, where the presence of a resonance aggravates the difficulty of reliably extrapolating $S(0)$.

Another difficulty which becomes increasingly important for low energies arises from atomic screening in laboratory experiments. The experimentally measured cross-section, σ_{exp}, is not the bare-nucleus cross-section, σ_0, but is increased by a factor

$$f_{\mathrm{e}}(E) = \sigma_{\mathrm{exp}}(E)/\sigma_0(E)$$

due to the screening of the nuclear charges by non-stripped electrons of the colliding ions [13]. To determine the relevant cross-section for the Sun from the bare-nucleus cross section, the enhancement caused by Debye–Hückel screening in the solar plasma must be taken into account [80, 81, 92].

Table 2 shows the current best estimates for the astrophysical S-factors.

Table 2. The solar fusion reactions. Astrophysical S-factors for the solar pp chains and CNO cycle (adapted from [5]), percentage of the chain terminations (i.e. per ^{4}He nucleus produced via the respective cycle) in which the respective reaction is involved, neutrino energy, and contribution Q to the solar energy generation of 26.7 MeV per ^{4}He nucleus produced [15].

Reaction	$S(0)$ (keV b)	Termination (%)	E_ν (MeV)	Q (MeV)
p(p, $e^+\nu$)^{2}H	$4.00(1 \pm 0.01^{+0.02}_{-0.01}) \times 10^{-22}$	100	$\leqslant 0.422$	1.442
p(pe^-, ν)^{2}H		0.4	1.442	1.442
^{2}H(p, γ)^{3}He		100		5.494
^{3}He(^{3}He, 2p)^{4}He	$(5.4 \pm 0.04) \times 10^{-3}$†	85		12.86
^{3}He(^{4}He, γ)^{7}Be	0.53 ± 0.05	15		1.586
^{3}He(p, e + ν)^{4}He	2.3×10^{-20}	2×10^{-5}	$\leqslant 18.8$	19.795
^{7}Be(e^-, ν)^{7}Li		15	0.862(90%)	0.862
			0.384(10%)	0.384
^{7}Li(p, α)^{4}He		15		17.347
^{7}Be(p, γ)^{8}B	$0.019^{+0.004}_{-0.002}$	0.02		0.137
^{8}B(, $e^+\nu$)^{8}Be*		0.02	$\leqslant 15$	17.980
^{8}Be*(, α)^{4}He		0.02		
^{14}N(p, γ)^{15}O	$3.5^{+0.4}_{-1.6}$			7.297
^{16}O(p, γ)^{17}F	9.4 ± 1.7			7.297

† The measured value $S(E_0)$ at the Gamow peak energy $E_0 = 21.4$ keV [94].

According to equation (7), apart from the astrophysical S-factors, the reaction rates and thus also the individual neutrino branches depend on the local element densities n_x. Particularly important in this context are the local densities of ^{1}H, ^{3}He, and ^{4}He. In the reference solar models, local equilibrium, corrected for element diffusion and gravitational settling of He towards the solar core, is assumed. This assumption has been validated in helioseismological measurements, whereas non-standard solar models[7] which *ad hoc* introduce strong mixing in the solar core to achieve non-equilibrium local element distributions [44] (mainly a local ^{3}He excess in the inner core in order to suppress the pp-II/pp-III chains; cf. figure 2) have been disproved. The same applies to models which assume rapid core rotation or strong trapped magnetic fields to counterbalance gravity, resulting in lower core temperatures and thus lower neutrino fluxes.

The neutrinos emitted in several steps of the pp cycle are referred to as pp, pep, ^{7}Be, ^{8}B, and hep neutrinos, according to the respective production reaction. Altogether 90% of the entire neutrino flux is believed to be pp neutrinos originating from the initiating reaction. They exhibit a continuous spectrum with an end-point of only 422 keV, which makes them the most difficult species to detect.

The second-largest contribution is ^{7}Be neutrinos from electron capture on ^{7}Be, the dominating process at the vertex of the pp-II and pp-III chain; cf. figure 2. As both the ground state and an excited nuclear level of the daughter nucleus ^{7}Li can be populated, the ^{7}Be-neutrino spectrum exhibits two discrete lines, at 862 keV (90%, ground state) and 384 keV (10%, excited level), respectively.

A line spectrum also characterizes pep neutrinos from the reaction p(e$^-$p, ν)^{2}H (not shown in figure 2(a)). The flux prediction for pep neutrinos is very accurate, as the process is closely linked to the pp reaction.

The opposite is the case for the high-energy ^{8}B neutrinos. Their prediction suffers from a large uncertainty in the astrophysical $S_{17}(0)$-factor [5]. There is an ongoing debate on the correct interpretation of experimental results from laboratory measurements of S_{17} and their low-energy extrapolation.

Not at all well determined, in addition, is the highest-energy neutrino branch: hep neutrinos from the pp-IV chain. The reason is the lack of low-energy measurements of the respective S-factor. Instead one has to infer $S_{31}(0)$ from measurements of thermal neutron capture on ^{3}He, a procedure which suffers from substantial uncertainties associated with the nuclear matrix elements involved. A recent assessment of the experimental and theoretical situation has revealed that even a factor-of-ten uncertainty for the flux prediction cannot be firmly rejected on the basis of the existing knowledge.

In contrast to the pp chains, the CNO cycle depicted in figure 3 is considered not to play a particularly prominent role for solar energy generation. It contributes only about 1.5% to the solar luminosity and 2% to the integral neutrino flux, according to solar model predictions[8]. From the reaction network, CNO-I dominates by far, and here it is the reaction ^{14}N(p, γ)^{15}O which constitutes the bottleneck at solar temperatures. It is assumed that the CNO cycle has not yet reached equilibrium and ^{14}N is still being accumulated [35]. This leads to a higher flux of ^{13}N neutrinos, compared to the ^{15}O neutrino flux; cf. table 1.

As depicted in figure 2(b), CNO neutrinos exhibit continuous spectra, with typical energies

[7] Almost all non-standard models were proposed in order to provide an 'explanation' of the observed solar neutrino flux deficits. In order to reconcile solar neutrino fluxes being substantially lower than predicted by the reference models, they have to rely upon *ad hoc* assumptions for input parameters and/or physical processes which are not generally considered to correctly describe the Sun.

[8] However, it is interesting to note that the CNO cycle would constitute the dominant process if the solar core temperature were only slightly higher, $T_c \gtrsim 3 \times 10^6$ K [124, 137].

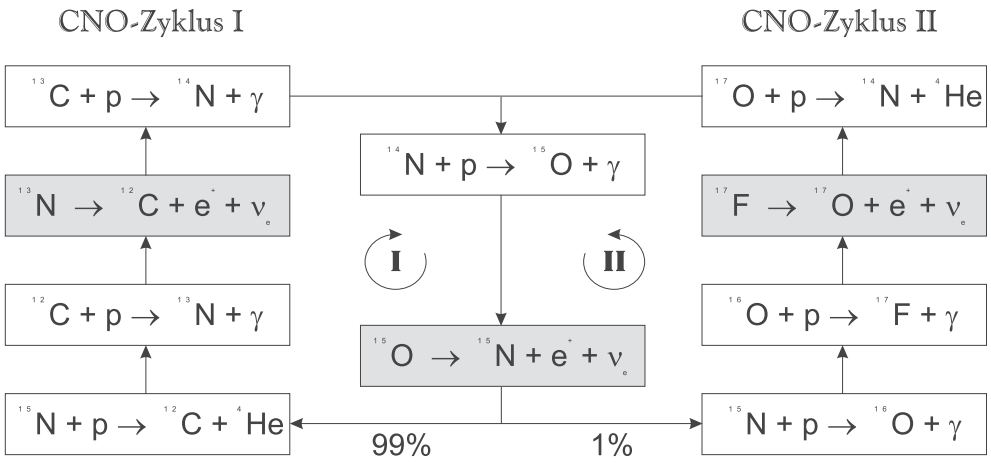

Figure 3. The CNO cycle, which contributes about 1.5% to the energy release of the Sun, gives rise to the continuous spectra of ^{13}N and ^{15}O neutrinos.

in the ^{7}Be range. In addition, the integral CNO neutrino flux is not substantially lower than that of ^{7}Be neutrinos:

$$\int \frac{\mathrm{d}\Phi(\mathrm{CNO})}{\mathrm{d}E}\,\mathrm{d}E \simeq 0.2 \sum_{i=384,861\,\mathrm{keV}} \Phi_i(^{7}\mathrm{Be}).$$

Compared to the effort invested in precise S-factor determinations of pp-cycle reactions, cross-sections for the CNO reactions are much less accurately known [5]. However, the LUNA collaboration has upgraded the accelerator utilized at Gran Sasso Underground Laboratory to determine the ^{3}He–^{3}He cross-section [93] for investigating CNO reactions at stellar energies [95].

3.3. Uncertainties and accuracy of neutrino flux predictions

For the interpretation of solar neutrino experiments, precise and trustworthy flux predictions constitute an important prerequisite. This applies not only to the integral flux, but, in particular, also to the individual neutrino branches. In the following we will discuss the influence of uncertainties associated with the input parameters and idealized physical concepts of the solar models on the neutrino flux predictions.

3.3.1. Opacities. The radiative opacity coefficients, determining how efficiently photons can transport energy from the solar centre outwards to the surface, are important for computations of the radial temperature profile and thus the relative contributions of the four subchains of the pp cycle. It was found empirically [15, 34] that the flux of ^{7}Be neutrinos, $\Phi(^{7}\mathrm{Be})$, scales approximately as T_c^{8}. Not surprisingly, boron neutrinos are even more sensitive, $\Phi(^{8}\mathrm{B}) \propto T_c^{18}$, whereas pp neutrinos, due to the luminosity constraint, remain essentially unaffected by variations of the core temperature T_c.

On the basis of improved determinations of the photospheric abundances of several elements [78], the OPAL opacity tables were updated in 1996 [101]. As for the intermediate region of the Sun, high-precision helioseismological observations have meanwhile allowed the probing of the influence on the speed of sound caused by changes of the opacity coefficients

exceeding a few per cent; the excellent agreement between the predicted and measured c_s-profiles supports the updated opacities. Neutrino flux predictions, except to some extent the highly temperature-dependent ^{8}B and hep fluxes, can be considered robust with respect to opacity uncertainties.

3.3.2. Nuclear cross-sections and atomic screening. As already mentioned above, uncertainties associated with nuclear cross-sections arise mainly from two sources:

- Laboratory measurements are—except for the ^{3}He–^{3}He reaction—performed in an energy range which is typically one order of magnitude higher than the Gamow region for the respective reaction in the solar core. Extrapolations of the data to solar energies introduce an uncertainty. The uncertainty is particularly serious for the ^{7}Be–p reaction, i.e. $S_{17}(0)$, giving rise to the ^{8}B neutrinos. Low-energy data for S_{17} are entirely lacking, direct laboratory measurements suffer from a resonance at 0.6 MeV, and results from an indirect method exploiting Coulomb dissociation of ^{8}B in the strong Coulomb field of a Pb nucleus [112] which does not suffer from the resonance are only in marginal agreement with the direct measurements. In addition, the assessment of systematics in the S_{17}-measurements has recently been criticized, which, if the criticism is justified, could indicate a need to increase the uncertainty of S_{17} with respect to the published values [11, 95]. According to the empirical scaling law $\Phi(^8\mathrm{B}) \propto S_{17}S_{34}^{0.81}S_{33}^{-0.4}$ [15], this would reduce the accuracy of the flux prediction for ^{8}B neutrinos.
- Screening corrections become increasingly important at low energy. As mentioned above, the cross-section determined in laboratory experiments is enhanced by a factor $f_e(E) > 1$ with respect to the bare-nucleus cross-section, due to the presence of bound atomic electrons. After several years' controversy, the problem of reliably calculating these enhancement factors $f_e(E)$ seems to be now largely dealt with, at least for atomic targets [5, 94, 104]. A reliable assessment of atomic screening is particularly important for the determinations of S_{33}, as the LUNA measurements extend down to 16.5 keV [29], corresponding to the lower edge of the Gamow peak.

3.3.3. Plasma screening. Electron screening in the solar plasma enhances the fusion rates by diminishing the effective repulsive Coulomb barrier with respect to bare nuclei [125]. The reference solar models employ a modified Debye–Hückel description to account for this [80, 81, 92]. There has been an extensive debate on the correct description for solar plasma screening, i.e. whether classical weak screening, intermediate screening [77], or dynamical screening is more appropriate (cf. [5, 35, 137] and references therein). More recent theoretical investigations seem to largely tend towards weak screening [5]. In summary, however, we do not consider the treatment of plasma screening to introduce a non-negligible uncertainty for neutrino flux predictions, except perhaps for the high-energy ^{8}B-neutrino branch.

3.3.4. Other sources of uncertainty. Other input to the calculations comprises the more or less idealized descriptions of physical processes considered relevant for the Sun—or their omission. For these issues also, new determinations of photosphere element abundances and the precision measurements of helioseismology have served to clarify the scenario.

Helium and heavy-element diffusion, i.e. gravitational settling towards the solar centre, has been proven to be non-negligible and is now generally taken into account in the reference solar models. The inclusion of diffusion has an effect on neutrino flux predictions, mainly for the high-energy ^{8}B neutrinos.

The sensitivity of solar p-mode frequencies on the equation of state leads to the conclusion that the appropriate prescription for the solar plasma is reasonably well understood and that associated uncertainties are under control.

Numerics could be important as regards interpolations of the tabulated radiative opacities and the numerical treatment of convection in the outer regions of the Sun, as both influence the solar temperature profile. However, Schlattl *et al* [127, 128] have constructed a solar model with an improved numerical treatment and found their results to agree with the reference models. We therefore do not consider this issue to introduce any non-negligible systematics for the flux predictions.

In conclusion, there remain two main sources for uncertainties in neutrino flux predictions. Firstly, though helioseismology has led to major improvements, it is still desirable to have more accurate radiative opacities. Secondly, several of the nuclear reaction cross-sections need to be measured at energies as low as possible in order to arrive at more reliable values for the astrophysical S-factors. In particular, the knowledge of the cross-section factors for S_{17}, S_{34}, and S_{31} needs to be improved. In parallel to low-energy measurements along the LUNA lines, a better theoretical understanding of screening effects in both the laboratory reactions and the solar plasma is desirable.

4. Solar neutrino detection

In this section we describe general principles for the detection of solar neutrinos. The absorption or scattering processes of neutrinos with matter via weak interaction in the relevant energy range are discussed and numerical values for the cross-sections are given. We emphasize the importance of charged-current (cc) as well as neutral-current (nc) interaction for the measurement of the flavour content of solar neutrinos. In addition, we discuss the basic technical items which are indispensable to the feasibility of solar neutrino experiments, emphasizing the important issue of background suppression. In section 4.4, operating experiments and their results will be presented, whereas the potential for upcoming projects to pinpoint neutrino masses and mixing angles will be discussed in section 6.

4.1. Charged-current and neutral-current detection

Weak interaction is mediated by exchange of either charged $W^{\pm}$ or neutral Z^0 bosons. These cases are referred to as charged-current (cc) and neutral-current (nc) interaction, respectively. Charged-current reactions of neutrinos ν_l ($l = e, \mu, \tau$) with nuclei can be described as 'inverse beta decays' of the form

$$\nu_l + {}^{A}_{Z}\mathrm{X} \rightarrow l^- + {}^{A}_{Z+1}\mathrm{Y}$$

where the nuclei X and Y have equal atomic number A, but differ in their electric charge Z by one unit. The energy threshold Q is given by $Q = m_Y + m_l - m_X$ for ground-state transitions, where m_i ($i = l, X, Y$) are the masses of the particles involved in the inverse beta decay and a possible neutrino mass is neglected. In transitions to excited states, the additional energy has to be taken into account. For electron neutrinos ν_e, allowed reactions with Q-values in the MeV range and even below exist. Since the maximum energy of solar neutrinos $E_\nu^{\max} \approx 15$ MeV, detection of solar ν_e with nuclear targets using charged-current interaction is possible. One example is $^{71}\mathrm{Ga} + \nu_e \rightarrow {}^{71}\mathrm{Ge} + e^-$ which is used in the radiochemical gallium experiments GALLEX/GNO [67, 71] and SAGE [3] with a threshold of 233 keV; cf. section 4.4.

If the flavour of solar neutrinos is changed during their journey from the interior of the Sun to the Earth, for example due to oscillations as described in section 2, the detection of

those new flavours by the reaction above is forbidden kinematically. The reason for this is the large masses of the corresponding charged leptons, $m_\mu = 106.95$ MeV and $m_\tau = 1777$ MeV, which exceed $E_\nu^{\max}$ by far.

However, neutral-current interaction is possible for all neutrino flavours. Hence, comparison of observed rates in neutral-current as well as charged-current reactions allows one in principle to measure the flavour content of solar neutrinos arriving at the Earth and to determine whether neutrino oscillations do occur or not in the respective energy range. This is the aim of experiments which started data taking recently or are projected for the near future.

Neutral-current interaction contributes to elastic neutrino–electron scattering:

$$\nu + \mathrm{e}^- \rightarrow \nu + \mathrm{e}^-$$

which is used in the SUPERKAMIOKANDE [133] and SNO [50] experiments for the detection of highly energetic ^{8}B neutrinos. The same reaction will be used in the future BOREXINO project [31] to examine the monoenergetic ^{7}Be neutrino flux at $E_\nu = 861$ keV.

The scattering of ν_e is due to both cc and nc interaction, whereas the $\nu_{\mu,\tau}$ scatter only via the nc reaction. Hence, if the flavour of solar ^{7}Be neutrinos was converted almost totally from ν_e to ν_μ or ν_τ when arriving at the Earth, the counting rate in BOREXINO would be reduced by a factor of $\approx$4, but still remain observable. In contrast, as ν_μ and ν_τ produced by oscillations from solar ν_e cannot interact via the cc reaction, for strongly converted ^{7}Be neutrinos the capture rate on nuclei would be suppressed dramatically. Inverse beta decays with such low Q-values, apart from those of ^{71}Ga and ^{37}Cl, are known [118] and it is the aim of LENS [107] (cf. section 6.5) to perform a cc measurement which is—in contrast to the radiochemical gallium experiments—energy dispersive.

Another example of nc reactions used in solar neutrino experiments is the dissociation of deuterium, $\nu + {}^2\mathrm{H} \rightarrow \nu + \mathrm{p} + \mathrm{n}$, which occurs at a threshold of 2.2 MeV. This reaction is used in the SNO experiment [50] to investigate possible flavour conversion of solar ^{8}B neutrinos by comparing the measured counting rate with that of the cc reaction $\nu_\mathrm{e} + {}^2\mathrm{H} \rightarrow \mathrm{e}^- + \mathrm{p} + \mathrm{p}$.

Both examples show an experimental attempt by comparing cc and nc reactions to measure the flavour content of solar neutrinos arriving at the Earth. If these experiments show a significant deviation from a pure ν_e-flux of solar neutrinos, the hypothesis of neutrino oscillation will be unequivocally proven. In addition, it will also be possible to examine fundamental neutrino properties connected with oscillations, namely the mass difference and the mixing amplitude involved. How these questions will be investigated experimentally is described in sections 5 and 6.

4.2. General detector requirements

As neutrino detection is always based on weak interaction, the detection cross-section in the energy range relevant for solar neutrinos is tiny. For instance, the numerical value for elastic neutrino–electron scattering is $\sigma(\nu_\mathrm{e}, \mathrm{e}^-) \simeq 9.5 \times 10^{-45} (E_\nu/\mathrm{MeV})\ \mathrm{cm}^2$, which is $\approx$20 orders of magnitude lower than typical cross-sections of electromagnetic scattering processes. These low values make solar neutrino detection very difficult and require large target masses to be utilized in order to obtain reasonable event rates. Experiments use detector masses from the $\approx$100 t mass range up to the kiloton scale.

Since cosmic radiation, in particular high-energy muons, can produce background events which are indistinguishable from neutrino signals, all solar neutrino experiments are located deep underground. The main background sources due to cosmic muons originate from spallation processes. High-energy muons may produce electromagnetic and hadronic showers, generating radioactive nuclei which may mimic neutrino signals in the detector. The typical

reduction factors of muon fluxes achieved in underground laboratories are in the range of $\approx 10^6$ for a rock overburden of ≈3000 m.w.e. (metres of water equivalent).

In addition, particle and gamma radiation is present due to ubiquitous natural radioactivity contaminants such as ^{238}U, ^{232}Th, and ^{40}K. Due to their high mobility, the noble gases ^{222}Rn (produced in the decay series of ^{238}U) and the anthropogenous fission product ^{85}Kr (from atomic bomb tests) are jeopardizing particularly low-energy experiments. Hence, solar neutrino experiments usually have to be shielded against this radiation, and detector materials need to be selected carefully in terms of radiopurity.

4.3. Solar neutrino experiments: an overview

Solar neutrino detection is realized in two ways: either radiochemically or in energy-dispersive measurements. The former method is based on the chemical extraction of the small number of nuclei produced in inverse beta reactions during an exposure period of typically some weeks from a large amount of target (typically in the 100 ton range). After extraction, the back-decay of those nuclei is observed. This concept was realized for the first time in the Homestake ^{37}Cl experiment [49], which measures solar neutrinos via the reaction $\nu_e + {}^{37}\mathrm{Cl} \rightarrow e^- + {}^{37}\mathrm{Ar}$ at an energy threshold of 814 keV, giving access to the solar ^{8}B branch and, to some extent, to ^{7}Be neutrinos. About twenty years later, the radiochemical GALLEX and SAGE experiments began to measure the integral flux of all solar neutrino branches using ^{71}Ga as target isotope. Here, the energy threshold is 233 keV, and for the first time pp neutrinos produced in the initiating solar fusion reaction $p + p \rightarrow \nu_e + {}^2\mathrm{H}$ could be detected. Since 1998, GALLEX has continued as the Gallium Neutrino Observatory GNO.

Radiochemical experiments exhibit the potential to detect even the lowest-energy neutrino branch, pp neutrinos. The information on neutrino energy, however, is lost. Instead, a radiochemical experiment constitutes something like a 'fixed-threshold counting device'. Therefore, identification of the contribution of the individual neutrino branches to the detected signal cannot be accomplished in one single experiment alone, but requires information from several radiochemical detectors with different thresholds.

Direct information on E_ν is provided from energy-dispersive experiments. However, the energy threshold of the running and near-future projects is too high for assessing pp neutrinos. For the first time, the energy-dispersive technique was realized in the water Cherenkov detector KAMIOKANDE [91] and later in its upgrade SUPERKAMIOKANDE. The detection technique is elastic neutrino–electron scattering at an energy threshold of ≈5 MeV (for SUPERKAMIOKANDE), allowing only the high-energy part of the ^{8}B spectrum to be investigated. The reason for this high threshold is the formidable background from natural radioactivity arising in the ≈MeV region.

The other operative energy-dispersive experiment, SNO, uses heavy water as target material. Its energy threshold is comparable to that of SUPERKAMIOKANDE.

A new detection concept, using large-volume, high-purity liquid scintillators for measurement of neutrino–electron scattering, allows investigation of neutrinos in the region around 1 MeV. This is possible due to the much higher light yield of scintillators, compared to that in the Cherenkov technique. The most advanced projects are BOREXINO and KAMLAND.

Table 3 lists running solar neutrino experiments as well as some projects which will start data taking in the future. Up to now, six different experiments have delivered data on solar neutrinos. Interestingly, in all cases, the measured flux is significantly lower than expected from solar model computations, establishing the so-called solar neutrino puzzle. In the following we will cover these experiments in detail and discuss the impact of their results on different solutions to the solar neutrino puzzle.

Table 3. A list of solar neutrino experiments according to their reaction mechanism, energy threshold $E_{\rm thr}$ in MeV, status (data available), measured counting rate in events per day, expected counting rates from the reference solar model (events/day), potential for energy-dispersive (ed), charged-current (cc), and neutral-current (nc) measurements. SUPERKAMIOKANDE (SK), SAGE, GNO, SNO, and the Cl experiment are taking data. BOREXINO, KAMLAND and the iodine experiment are under construction, LENS is a project still in an early development phase.

Experiment	Reaction	$E_{\rm thr}$	Data	Rate	Solar model	ed	cc	nc
^{37}Cl	$\nu_e(^{37}\mathrm{Cl}, ^{37}\mathrm{Ar})e$	0.814	×	0.5	1.5		×	
GALLEX/GNO	$\nu_e(^{71}\mathrm{Ga}, ^{71}\mathrm{Ge})e$	0.233	×	0.8	1.5		×	
SAGE	$\nu_e(^{71}\mathrm{Ga}, ^{71}\mathrm{Ge})e$	0.233	×	0.8	1.5		×	
SK	$\nu e \rightarrow \nu e$	≈ 5	×	13.5	28.5	×	×	×
SNO	$\nu_e{}^2\mathrm{H} \rightarrow \mathrm{epp}$	≈ 5	×	?	24.1	×	×	
	$\nu\mathrm{D} \rightarrow \nu\mathrm{pn}$	2.2			7.1	×		×
	$\nu e \rightarrow \nu e$	≈ 5	×	?	3.3	×	×	×
BOREXINO	$\nu e \rightarrow \nu e$	≈ 0.4			59.0	×	×	×
KAMLAND	$\nu e \rightarrow \nu e$	≈ 0.5			112.6	×	×	×
^{127}I	$\nu_e(^{127}\mathrm{I}, ^{127}\mathrm{Xe})e$	0.789			?		×	
LENS	$\nu_e({}^A_Z\mathrm{X}, {}^A_{Z+1}\mathrm{Y})e$	$\gtrsim 0.3$			≈ 0.5	×	×	

4.4. Operating experiments and their results

4.4.1. Chlorine. For more than 20 years, the radiochemical ^{37}Cl detector operated since 1968 by Davis *et al* [48, 49] in the Homestake gold mine in Lead, South Dakota, USA, at a depth of 4200 m.w.e.[9] was the only active solar neutrino experiment. The experiment employs 615 tons of C_2Cl_4 (^{37}Cl natural abundance: 24.2%) as target material for the inverse beta-decay reaction $^{37}\mathrm{Cl} + \nu_e \rightarrow {}^{37}\mathrm{Ar} + e^-$, which has an energy threshold of 814 keV. The experiment is mainly sensitive to ^{8}B neutrinos from the pp-III chain, and, to a smaller extent, to ^{7}Be and CNO neutrinos (cf. table 4).

Table 4. The spectral response of the chlorine experiment, according to the reference solar model [19]. The unit SNU (solar neutrino unit) is defined as 1 SNU = 1 neutrino capture reaction/10^{36} target atoms s^{-1}.

	pp	pep	^{7}Be	^{8}B	^{13}N	^{15}O	Integral
$\langle\sigma\Phi_\nu\rangle$ (SNU)	0	0.2	1.15	5.9	0.1	0.4	$7.7^{+1.2}_{-1.0}$

Only a fraction of ± 0.2 SNU of the total error for the SNU prediction is associated with the neutrino capture cross-section which is dominated by a transition to an isobaric analogue state at 5 MeV and can be quite accurately determined from the beta decay of ^{37}Ca. The dominant contribution to the error, in contrast, comes from the flux prediction of ^{8}B neutrinos.

The few atoms of ^{37}Ar produced by neutrino interaction in the target of the Homestake experiment are extracted every few months by purging the target with helium, and added to the counting gas of a miniaturized, low-background proportional counter, where the electron capture (EC) decay of ^{37}Ar (half-life 35 d) is detected during a several-month counting period.

[9] To allow a straightforward comparison of the shielding properties for different underground sites, the attenuation of cosmic rays is given in terms of *metres of water equivalent* (m.w.e.).

The offline analysis employs a maximum-likelihood technique [38] for analysing the time series of the candidate events.

Between 1970 and 1994 the Homestake experiment accumulated a statistics of 108 solar runs. The integral result, $(2.56 \pm 0.16(\text{stat.}) \pm 0.15(\text{syst.}))$ SNU [39,105], is significantly lower than the solar model predictions, representing a factor-of-three (or $>5\,\sigma$, when combining in quadrature the experimental and flux prediction errors) neutrino deficit. As the experimental result is already far more accurate than the solar model prediction, to gain further statistical significance, improvement of, in particular, the determination of the astrophysical S_{17}-factor is an unavoidable requirement (cf. section 3).

However, a qualitatively different situation is encountered when exploiting the real-time potential of the experiment (with the time resolution given by the duration of target exposure) for probing potential time variations of the solar neutrino flux (cf. section 4). Here the limitation arises from the large statistical errors associated with the results of individual runs. Therefore, though time variations of the observed neutrino flux—more precisely an anticorrelation with the Sun spot number which would be indicative for a neutrino magnetic moment—have been claimed to accommodate the data, the statistics is not sufficient for rejecting the standard hypothesis of time constancy; in contrast, the question continues to remain an arena for debate.

4.4.2. KAMIOKANDE. The solar ^{8}B-neutrino flux was measured in the KAMIOKANDE water Cherenkov detector, installed in the Kamioka mine in Japan. Data were accumulated from January 1987 until February 1995, covering almost an entire solar cycle.

The detector, a cylindrical tank 15.6 m in diameter and 16.1 m in height, contained about 3000 tons of pure water in total. Its inner 680 tons were used as a fiducial volume for the solar neutrino analysis. Neutrino detection employed elastic neutrino–electron scattering, the Cherenkov light of back-scattered electrons being viewed by 948 photomultiplier tubes (providing a 20% coverage in total).

Major cuts in data reduction comprise rejection of muons with the help of an outer veto counter, rejection of events due to external γ-radiation and neutrons by choosing a fiducial volume, and rejection of muon-induced spallation signals and decay electrons from stopped muons by delayed anticoincidence methods. The energy threshold achieved was $\approx$7 MeV. Hence, KAMIOKANDE was sensitive to the high-energy part of the solar ^{8}B-neutrino spectrum only. As at these energies the angular distribution of the scattered electrons is significantly peaked in the forward direction, directional information could be used to further separate neutrino events from background signals. With these cuts a data reduction by a factor of $\approx 1/1.5 \times 10^5$ was obtained and a clear neutrino signal from the Sun's direction is visible.

The KAMIOKANDE collaboration has published results for a total observation time of 2079 days [96]. The measured ^{8}B neutrino flux is $\phi_\nu = (2.82 \pm 0.19(\text{stat.}) \pm 0.33(\text{syst.})) \times 10^6$ cm^{-2} s^{-1} which is only about 49%–64% of the predictions from different reference solar models [16,138]. This deficit is significantly larger than the total uncertainties from both theory and experiment. The number for ϕ_ν was calculated under the assumption of a pure ν_e-flux, taking into account the charged-current as well as neutral-current contributions to the total cross-section. Analysis for time variations including the separation of day and night records was performed in order to test certain neutrino-mixing parameters. However, no significant differences in the data were found.

4.4.3. SUPERKAMIOKANDE. The SUPERKAMIOKANDE imaging water Cherenkov detector is the successor of the KAMIOKANDE experiment. About 50 kilotons of ultrapure water is used as the Cherenkov medium where a fiducial volume corresponding to 22.5 kt is

used as the solar neutrino target. This is an upscale with respect to KAMIOKANDE by a factor of ≈33, and the signal rate is of the order of about 10 per day. Data taking started in April 1996 with an electron energy threshold of 6.5 MeV. Meanwhile the threshold for the neutrino energy was reduced to 5.0 MeV [135].

In order to achieve this threshold, special care was taken in background suppression. As radioactivity from radon is the dominant background contribution, radon is removed from the water to a limit of 5.7 mBq m^{-3} [136] which implies an improvement in radiopurity by a factor of ∼100 compared to the KAMIOKANDE detector.

Precise energy calibration is essential for measuring the energy spectrum of the recoil electrons. In SUPERKAMIOKANDE an electron linear accelerator is used for this purpose. The Linac injects downward-going monoenergetic single electrons into the detector at an energy which can be tuned between 5 and 16 MeV [56]. The calibration utilizes data from the Linac at eight different positions inside the fiducial volume. The uncertainty in the beam energy is 0.55% at 6 MeV and 0.3% at 10 MeV. The absolute energy scale is monitored for stability and cross-checked using decay electrons from stopped muons, cosmogenically created radionuclides, and a Ni(n, γ)Ni source.

Data reduction in SUPERKAMIOKANDE is achieved via rejecting external gamma rays and muon-induced spallation events. The data sample is divided into energy bins of width 0.5 MeV from the threshold up to 14.0 MeV and into one additional bin combining data from 14.0 to 20.0 MeV. By analysing the angular distribution with respect to the position of the Sun for each energy bin, the number of solar neutrino interactions is extracted. Figure 4 shows the

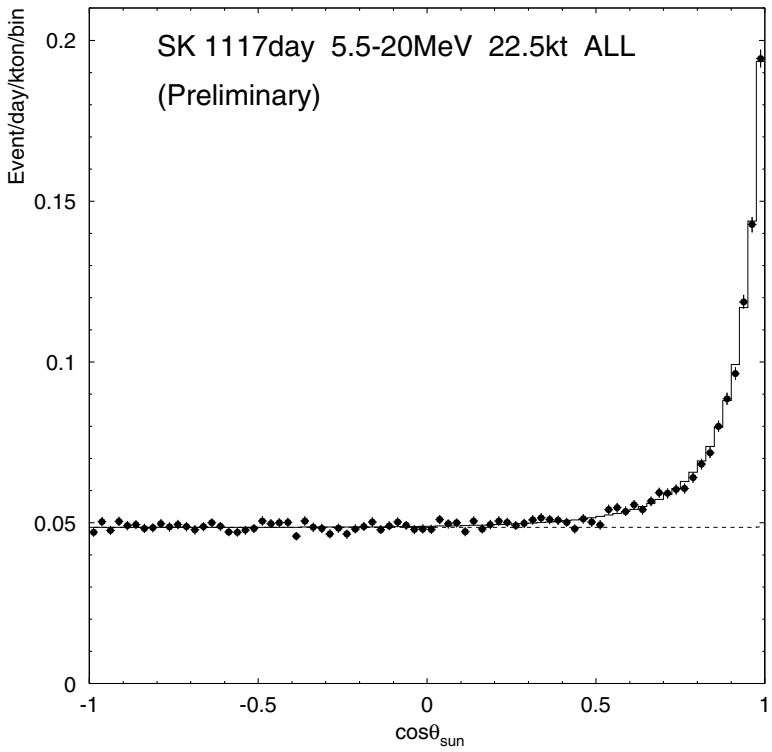

Figure 4. Angular distribution of the SUPERKAMIOKANDE solar neutrino data [135]. The data clearly point towards the Sun.

combined angular distribution of these events. The region far from the forward peak provides a measure of the background. It is found to be very close to being isotropic; only slight directional anisotropies are found which may introduce an uncertainty of 0.1% in the reported neutrino flux.

The background and the expected angular distributions of the solar neutrino signal are incorporated into a maximum-likelihood analysis which yields the number of neutrino events. Taking into account the cross-section of the ν_e-interaction, a ^{8}B ν_e-flux of $\phi = (2.40 \pm 0.03^{+0.08}_{-0.07}) \times 10^6$ cm^{-2} s^{-1} for 1117 d of data taking between 31 May 1996 and 24 April 2000 is reported [135].

This is in agreement with the KAMIOKANDE data at a 1 σ level. Comparison with the expected value $\phi^{\text{theo}} = (5.15^{+0.98}_{-0.72}) \times 10^6$ cm^{-2} s^{-1} from the reference solar model [19] leads to the conclusion that the deficit in the solar ^{8}B flux which was already observed in KAMIOKANDE persists. However, the significance of the deficit is enhanced due to the substantial reduction in experimental uncertainty achieved in SUPERKAMIOKANDE.

The time behaviour of the measured flux shows very good agreement with the seasonal variation expected from the eccentricity of the Earth's orbit.

Due to the high statistics, it is possible to test neutrino oscillation parameters by comparing the shape of the measured recoil spectrum with that expected from a Monte Carlo simulation of the ^{8}B decay. The simulated events are passed through the same analysis cuts as the real data. In order to compare the shape of the measured recoil spectrum with the expected one, the ratio of the two classes is plotted for each energy bin in figure 5.

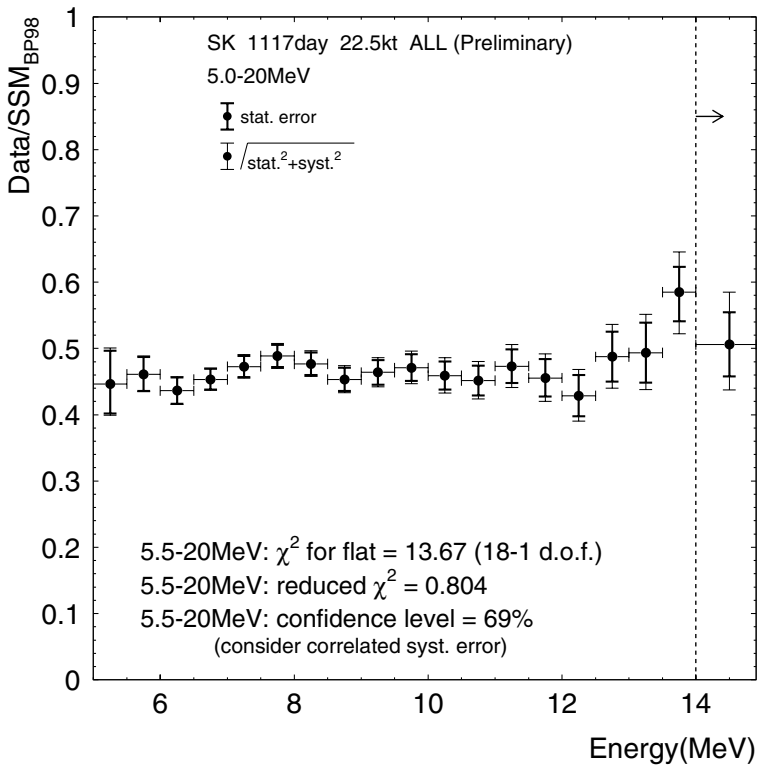

Figure 5. Normalization of the measured electron recoil spectrum to the one expected from ^{8}B decay, with the reference model [19] referred to for the flux prediction [135].

Though a slight deviation from a flat normalized shape is observed in the last high-energy bins, a χ^2-analysis of the entire spectrum shows agreement with the assumption of a flat shape [135].

The rate of solar neutrino production by the reaction ^{3}He+p $\rightarrow^4$ He+e$^+$+ν_e (hep neutrinos, end-point energy $\approx$16 MeV) contributes, according to the reference solar models, only a tiny fraction to the emitted flux. However, as discussed in section 3, the cross-section for the hep reaction is highly uncertain. The SUPERKAMIOKANDE collaboration deduces a limit of $\Phi(\text{hep})/\Phi^{\text{RSM}}(\text{hep}) < 13.2$ from the high-energy part of their observed spectrum above the ^{8}B end-point [135].

In part of the MSW scenario, a small enhancement of the solar neutrino flux during the night when the neutrinos pass the Earth is expected. The small-angle solution (cf. section 5) predicts an increase only when the neutrinos pass the core of the Earth which corresponds to a zenith angle between 140° and 180°, whereas the large-mixing solution favours an enhancement throughout essentially the entire night. The observed day–night asymmetry for 1117 days of measurement is $(D-N)/(D+N) = -0.034 \pm 0.022(\text{stat.})^{+0.013}_{-0.012}(\text{syst.})$ [135], where D and N are the counting rates during the day and night, respectively. Hence, the data slightly favour an enhancement during the night—however, only at a 1.3 σ level.

4.4.4. GALLEX and GNO. Neither the radiochemical ^{37}Cl experiment nor the water Cherenkov detectors KAMIOKANDE and SUPERKAMIOKANDE are able to detect the main bulk of neutrinos from the Sun: pp neutrinos from the initiating reaction of the solar fusion network, which, according to table 1, contribute about 90% of the integral flux.

At present and most probably also for the next decade, a radiochemical method exploiting the inverse β-decay reaction $^{71}\text{Ga} + \nu_e \rightarrow {}^{71}\text{Ge} + e^-$ will provide the only feasible way to access solar pp neutrinos. This reaction, proposed by Kuzmin in 1966 [100], exhibits an energy threshold as low as 233 keV, well below the end-point of the pp spectrum at 422 keV. The reference solar model predictions for the rate of neutrino capture on gallium agree very well, ranging between 124 SNU [30] and 129 SNU [19]. The reason is that the flux of pp neutrinos, as explained in section 3, is closely linked to the well determined solar luminosity. Thanks to their low threshold, the gallium experiments exhibit sensitivity to all solar neutrino branches, with the pp and ^{7}Be components contributing about 55% and 27% to the predicted capture rate. Table 5 lists the spectral response of a gallium neutrino detector.

Table 5. The spectral response of the gallium solar neutrino experiments: predicted capture rates for the solar neutrino branches, according to the reference solar model [19], and capture cross-sections on ^{71}Ga [18].

Component	Signal (SNU)	Cross-section (10^{-42} cm^2)	Cross-section uncertainty
pp	69.6	11.72	± 2.3%
pep	2.8	204	+17/−7%
Be	34.4	71.7	+7/−3%
B	12.4	2.4×10^4	+32/−15%
N	3.7	60.4	+6/−3%
O	6.0	113.7	+12/−6%
Integral	129^{+8}_{-6}		

GALLEX. The GALLEX experiment, operative from 1991 to 1998 [58, 67], employed 30 tons of natural gallium (isotope abundance of ^{71}Ga: 39.9%) in the form of 101 tons of aqueous $GaCl_3$ solution, acidified in HCl, as a neutrino target. The experiment, which performed neutrino observations from 1991 to 1997, is installed in the Gran Sasso Underground Laboratory (Laboratori Nazionali del Gran Sasso, LNGS) in Italy, which provides a rock overburden of 3300 m.w.e. to shield against cosmic rays.

After a standing time of typically ≈30 d, the neutrino-produced ^{71}Ge (of the order of 5–10 atoms, typically), present in the form of $GeCl_4$, which is highly volatile in an acidic environment, is extracted from the target solution (together with the ≈1 mg of stable isotope-pure germanium carrier that had been added at the beginning of the standing time) by purging the solution for about 12 h with 2500 m^3 of nitrogen. The $GeCl_4$ is absorbed in 50 l of water, and, after a series of concentration and purification steps, transformed to GeH_4. Together with xenon, the GeH_4 is filled into a miniaturized low-background proportional counter [146] and, after an initial calibration with a dedicated Ce fluorescence source [126, 141], counted for a minimum of 180 d in a well shielded spectrometer [90], in order to detect the x-rays and Auger electrons associated with the EC decay $^{71}\mathrm{Ge} + \mathrm{e}^- \rightarrow {}^{71}\mathrm{Ga} + \nu_\mathrm{e}$ (half-life $T_{1/2} = 11.4$ d [83]). In order to improve background suppression, not only is the energy of every candidate event recorded, but in addition, on several timescales, the digitized pulse shape. This makes an offline analysis possible, which can exploit the fact that background signals caused by environmental radioactivity or cosmic muons traversing the counter usually give rise to extended ionization patterns, whereas genuine ^{71}Ge decays cause characteristic compact signatures [6, 58]. From the time series of candidate events having survived all cuts in energy, pulse shape, and periods declared dead time, the ^{71}Ge activity and therefrom the SNU value are determined employing a maximum-likelihood method [38, 68].

In six years' running time, the GALLEX collaboration accumulated a statistics of 65 solar runs, subdivided into four data-taking periods (labelled as GALLEX-I to GALLEX-IV). The final combined result as well as the individual results for the four periods are listed in table 6. For a listing of the single-run results depicted in figure 6, we refer the reader to [68].

The overall GALLEX result is substantially lower than the prediction of any reference

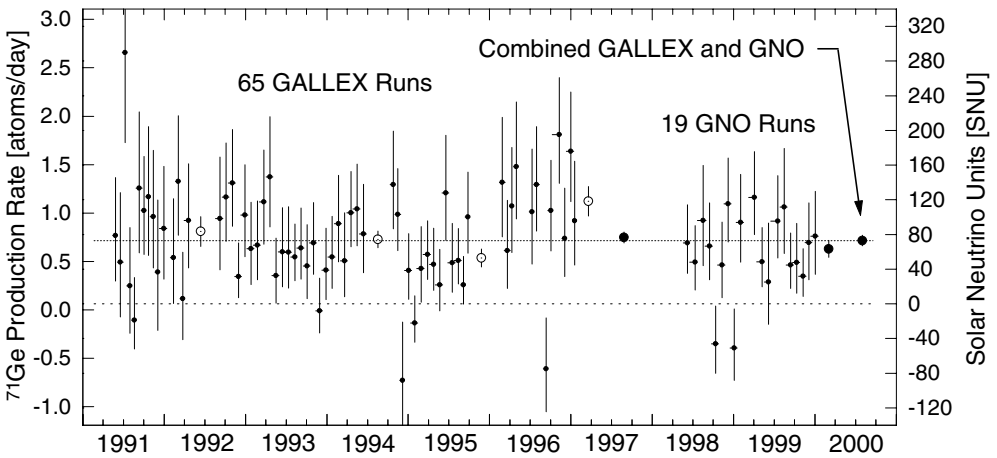

Figure 6. Individual run results of the GALLEX and GNO solar neutrino experiments (method I) [73]. The combined results for the four GALLEX data-taking periods and the overall combined result for all 65 runs are also marked, as well as the results for the subsequent GNO data taking, GNO-I.

Table 6. Results from the GALLEX solar neutrino experiment [68]. The two columns list the results obtained by the GALLEX collaboration by analysing their data with two independent methods (I: pulse rise time [58]; II: fit to the pulse [6]). Errors for the individual data-taking periods are statistical only. Both methods show good agreement in the final number, decisively indicating the presence of a statistically significant solar neutrino deficit for the integral flux, and supporting the interpretation that the large variation present for GALLEX-III and GALLEX-IV in method I is caused by a statistical fluctuation.

Period	Result, method I (SNU)	Result, method II (SNU)
GALLEX-I	83^{+19}_{-20}	73^{+18}_{-19}
GALLEX-II	76 ± 11	77 ± 10
GALLEX-III	54 ± 11	63 ± 11
GALLEX-IV	118 ± 19	105 ± 17
GALLEX-I to GALLEX-IV	$77.5 \pm 6.2^{+4.3}_{-4.7}$	$74.6 \pm 5.9 \pm 4.6$

solar model. This $>5\,\sigma$ effect, by itself, constitutes an indication for a particle physics solution, i.e. non-standard neutrino properties, as any alternative attempt to explain the observed deficit has failed to prove viable.

In this context it is important to note that the GALLEX collaboration has shown the entire detection procedure, including the neutrino capture on ^{71}Ga, to function as expected, by exposing their target twice to an intense, synthetic ^{51}Cr low-energy neutrino source of known activity ($(6.34^{+0.11}_{-0.16}) \times 10^{16}$ Bq and $(6.91^{+0.33}_{-0.21}) \times 10^{16}$ Bq for the two activations) [42,62,65,68] and by adding a known amount of ^{71}As to the target in order to produce ^{71}Ge *in situ* [66].

Figure 7 shows the results of the seventeen extractions performed with the target exposed to the ^{51}Cr neutrino source, normalized to the known activity A_{EoA} of the source at the end of neutron activation.

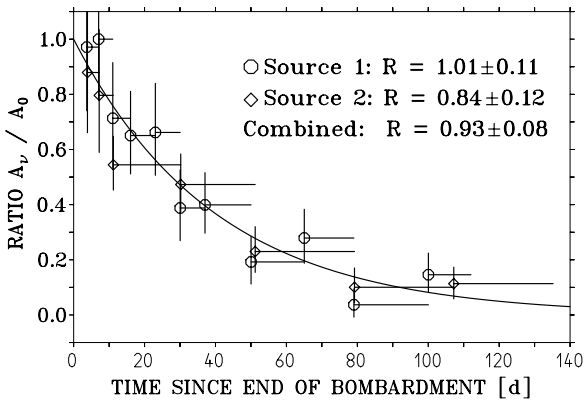

Figure 7. Results of the GALLEX Cr-neutrino-source experiments. The figure shows for every extraction the activity determined from the neutrino measurement, normalized to the known source strength at the end of neutron activation. The solid line does not depict a fit to the data but represents the expected behaviour resulting from the decay of the source with the 27.7 d half-life of ^{51}Cr. The horizontal bars at the data points indicate the lengths of the respective exposures.

The combined results of the two irradiations of the chromium source performed by the GALLEX collaboration are $R = A_\nu/A_{\mathrm{EoA}} = 1.01^{+0.12}_{-0.11}$ and $R = 0.84^{+0.12}_{-0.11}$, respectively, for analysis method I, and $R = A_\nu/A_{\mathrm{EoA}} = 0.99 \pm 0.11$ and $R = 0.85^{+0.11}_{-0.10}$ for method II, resulting

in an overall result of $R = 0.93 \pm 0.08$ (method I) and $R = 0.94 \pm 0.08$ (method II), both numbers in perfect agreement and consistent with 100% [65].

Supplementing the neutrino-source experiments, the GALLEX collaboration has performed, in view of the risk of contamination at the end of the solar neutrino campaign, an experiment employing ^{71}As which decays by EC and β^+ to ^{71}Ge. A known activity of ^{71}As (of the order of 10^5 atoms) was added to the target and, after a standing time allowing the ^{71}As to decay, the ^{71}Ge was extracted, treated by the standard chemical procedure and counted. Varying the experimental conditions in order to also test extreme scenarios, in all cases a quantitative recovery of 100% was observed. The good statistics allowed the pinpointing of the recovery yield to $(100 \pm 1)\%$ [66,97], excluding effects of hot chemistry which could in principle capture ^{71}Ge being produced in nuclear reactions into non-extractable components. Therefore, hence, this 'explanation' for the observed solar neutrino deficit is excluded. Knowing the chemistry to function perfectly, from the ^{51}Cr-neutrino-source experiments it is straightforward to conclude that the capture cross-section on ^{71}Ga cannot be accounted for by the observed 40% deficit either. In passing, we note that the GALLEX ^{51}Cr results have even been used to derive an estimate for the contribution of Gamow–Teller transitions to the 175 keV and 500 keV excited states to the neutrino capture cross-section on ^{71}Ga [65, 86, 88, 97].

Considering the accuracy of the reference solar models' predictions, in addition to the results from the ^{51}Cr and ^{71}As experiments, what remains as an explanation for the observed solar neutrino deficit is a particle physics solution. In section 5 we will discuss this issue in detail.

GNO. After the end of the GALLEX observations in mid-1997, the experimental set-up, which had been continuously in operation since 1990, was modernized and upgraded. Early in 1998, when all the activity introduced into the target with the arsenic tracer experiments had decayed away, solar neutrino measurements recommenced with the new set-up within the framework of the GNO experiment [71]. GNO (Gallium Neutrino Observatory) attempts performing a precision determination of the integral solar neutrino flux with an accuracy well beyond that of GALLEX, by monitoring solar neutrinos for a period of at least ten years, corresponding to one complete solar cycle. An increased accuracy for the measurement of the integral flux is essential for extracting separately the ν_e- and $\nu_{\mu,\tau}$-fractions of the individual neutrino branches from the cc and nc measurements being performed by the different experiments, as the gallium detector is the only feasible way of accessing pp neutrinos for at least the next decade.

In addition, GNO will also be able to increase its statistical significance for single-run measurements and small groupings of some few runs. This is important for exploiting the real-time potential of the experiment (with the time resolution determined by the duration of target exposure, which is constrained, by technical requirements, to minimally 12 h) for analyses of the time constancy of the neutrino flux. Physical scenarios predicting the flux to vary with time are, e.g., neutrino vacuum oscillations (cf. section 5 [142]), and a neutrino exhibiting a magnetic moment.

In order to fulfil the prerequisites for this goal, the GNO collaboration plans to increase its target mass from the present 30 tons to 66 tons (GNO-60) and later 100 tons (GNO-100), and, in addition, is developing improved low-level counting techniques (cf. [9, 10, 71]) with higher efficiency and better systematics. The aim is to achieve an error smaller than 4 SNU for the final cumulated result.

The first GNO extraction was done on 23 April 1998, with continuous routine operation of the experiment since then. Up to June 2000, altogether 24 solar runs have been performed. The first GNO result, including data from 19 runs, is 66 ± 12 SNU [72, 73], in good agreement

with GALLEX results. Merging the GNO runs with the GALLEX data set by performing a combined maximum-likelihood analysis results in 74 ± 7 SNU, with statistical and systematic errors combined in quadrature.

4.4.5. SAGE. Like GALLEX/GNO, the Russian–American SAGE detector[10], installed in the Baksan Underground Laboratory in the Caucasian Mountains, Russia, employs a gallium target to detect solar neutrinos via the cc inverse beta-decay reaction $^{71}\mathrm{Ga} + \nu_e \rightarrow {}^{71}\mathrm{Ge} + e^-$. In contrast to the case for GALLEX/GNO, however, the target, comprising between 50 and 57 tons of gallium, is utilized in metallic form (melting point 29.8 °C). Therefore, the chemical procedures for extracting ^{71}Ge from the target differ from that for GALLEX: extraction is performed by adding a mixture of deionized water, HCl, and H_2O_2 to the target, and heating and thoroughly stirring it, to produce an emulsion with the germanium entering into the oxide film covering the gallium droplets, where it can then be removed from the gallium, concentrated, and extracted into water in the form of $GeCl_4$. The subsequent experimental steps are similar to those of GALLEX/GNO, i.e. further concentration, purification, and synthesis of GeH_4 to be used in a mixture with Xe as the counting gas in miniaturized proportional counters. Like in GALLEX/GNO, counting is performed over a period of several months, in order to allow for a reliable estimate of the time-constant background counting rate. For counter calibration, done at regular intervals of about two weeks, standard ^{55}Fe and ^{109}Cd sources are used.

SAGE started solar neutrino recording in January 1990, and has been continuously operative since then. However, in spite of employing a target mass almost twice as large as that of GALLEX, the accuracy achieved so far is comparable to that of GALLEX. This is mainly due to the fact that in the initial phase of the experiment, background problems in counting prevented the collaboration from using L-peak data with 1 keV energy deposition (≈50% of the ^{71}Ge decays), i.e. only the 10 keV K events could be analysed. In addition, several extractions were entirely discarded due to potential uncontrolled systematics introduced by a gallium theft (altogether 2 t or 3.6% of the total mass) occurring in the period between November 1993 and June 1994. A detailed description of the experiment is given in [3].

The most recent published result from SAGE, comprising data from solar runs recorded between January 1990 and October 1999, is $(75.4^{+7.0}_{-6.8}(\mathrm{stat.})^{+3.5}_{-3.0}(\mathrm{syst.}))$ SNU [70], in good agreement with the GALLEX results, and substantially lower than any solar model prediction. Results for the individual data-taking periods are (81^{+20}_{-18}) SNU (SAGE-I, January 1990–May 1992), (79 ± 13) SNU (SAGE-II, September 1992–December 1994), and (72 ± 9) SNU (SAGE-III, March 1995–October 1999).

Also the SAGE collaboration has shown the experiment to work as expected by irradiating 13.1 tons of the target with a synthetic ^{51}Cr-neutrino source of known activity[11] ($A_{\mathrm{EoA}} = (517 \pm 6)$ kCi [1, 2]). The result of the ^{51}Cr experiment in SAGE is $R = A_\nu / A_{\mathrm{EoA}} = 0.95 \pm 0.12(\mathrm{exp.})^{+0.035}_{-0.027}(\mathrm{theo.})$, perfectly consistent with 100% [3].

SAGE is continuing to record the integral solar neutrino flux with a target mass of about 50 tons, complementing the GNO measurement with different systematics and, important for analyses of potential time variations, different extraction times. The collaboration plans to increase the target mass by ≈8 t by recovering the gallium that has been removed from the target in the course of the chemical extraction processes since the start of the experiment.

[10] The acronym SAGE stands for Soviet–American gallium experiment.

[11] The higher density of the metal target compared to the aqueous solution employed in GALLEX allows the achieving of the same event statistics with a substantially lower source activity.

4.4.6. SNO. The SNO experiment [50] is aiming to measure the flux of ^{8}B solar neutrinos with a heavy-water Cherenkov detector. SNO is situated 2000 m underground in the Creighton Mine near Sudbury, Canada [54].

The target is contained in an acrylic vessel 12 m in diameter. About 9500 photomultipliers, mounted on an open geodesic support structure, are used to deliver the signals from solar neutrino interactions. Each tube is 20 cm in diameter and is equipped with light reflectors, leading to a 70% coverage in total. Figure 8 shows the set-up of the experiment.

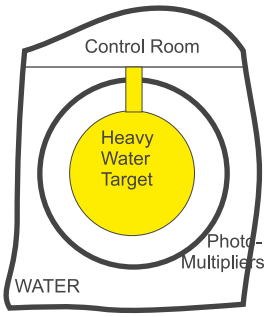

Figure 8. A schematic drawing of the SNO experiment. The neutrino target, 1000 tons of heavy water, is contained in an acrylic sphere, which is immersed in a light-water buffer to shield it from external radioactivity. Altogether 9500 photomultipliers are installed on a geodesic sphere surrounding the acrylic vessel.

In order to shield the target from external gamma rays, the heavy water is embedded in a light-water buffer which is contained in a barrel-shaped cavity. Water and radon permeation from outside is prevented by a thick polyurethane layer on the walls of the cavity.

The use of ^2H_2O as target offers the possibility of exploiting charged-current (cc) as well as neutral-current (nc) interactions. Three reactions are used for neutrino detection:

$$\nu_e + {}^2H \rightarrow e^- + p + p \qquad \text{(cc)}$$

$$\nu_x + {}^2H \rightarrow \nu_x + n + p \qquad \text{(nc)}$$

$$\nu_x + e^- \rightarrow \nu_x + e^- \qquad \text{(elastic scattering (es); cc + nc).}$$

The thresholds of the cc and the nc reaction on ^{2}H are about 6 MeV and 2.2 MeV, respectively. Therefore both reactions can only be used for detection of solar ^{8}B neutrinos. However, comparison of the reaction rates allows the simultaneous measurement of the flux of electron neutrinos (ν_e) and the flux independent of the flavour (ν_e, ν_μ, ν_τ). This information constitutes a signature for detection of neutrino oscillations to either another flavour ($\nu_e \rightarrow \nu_{\mu,\tau}$) or a sterile neutrino (ν_s). Direct neutrino spectroscopy is possible via the cc reaction by measuring the electron energy. Hence, spectral distortions due to oscillations might be detected, too, yielding independent information about the actual oscillation parameters. The energy resolution is expected to be ≈20% on average for ^{8}B neutrinos.

The disintegration of deuterium in the nc reaction is going to be detected by two methods. One way is to dope the water with $MgCl_2$, where Cl is used to capture the free neutrons liberated by the neutrino-induced deuteron break-up. Here the resulting 8.6 MeV gamma cascade will be detected. The second technique relies on ^{3}He-filled proportional tubes in the water target. Neutrons captured by ^{3}He provide a signal that is entirely independent of the photomultiplier array.

According to the reference solar model [19], SNO is expected to measure the following event rates: 8800 cc events/year, 2600 nc events/year ($MgCl_2$), 2300 nc events/year (^{3}He),

and 1200 es events/year. In addition, the electron energy spectrum of the cc reaction will be measured, which might be distorted by the presence of neutrino oscillations $\nu_e \rightarrow \nu_x$. It is important to note that the cc events can be separated from the es signals after reconstruction of the directionality of the recoil electron, as this differs for the two reactions.

The main background for these measurements are gamma and beta decays limiting the energy threshold for the cc reaction, and gamma rays with energies above 2.2 MeV capable of photodisintegration of deuterium via the reaction $\gamma + {}^2\mathrm{H} \rightarrow \mathrm{n} + \mathrm{p}$. The former background may compromise the detection of a potential spectral distortion, whereas the latter jeopardizes the nc measurement. Most of such background is likely to stem from decay products of the uranium and thorium chains. In order to set a limit to the background rate of one neutron per day, the mass concentrations of uranium and thorium in the heavy water have to be below 4.5×10^{-14} g g^{-1} and 3.7×10^{-15} g g^{-1}, respectively. In this case the expected signal-to-background ratio for the nc reaction would be at about 13. Design limits on the surrounding light water and the acrylic vessel are less stringent, and range in the 10^{-14} g g^{-1} and 10^{-12} g g^{-1} regions, respectively. All detector materials have been selected for low radioactivity and the construction proceeded in a clean-room environment. Special care was taken to prevent build-up of mine dust during construction of the acrylic vessel, as just 10 g of dust would be sufficient to account for a neutron rate equivalent to the nc signal. The collaboration succeeded in reaching the stringent radiopurity design limits.

Calibration of the detector is being accomplished using laser sources at different wavelengths and a diffuser ball which can be positioned almost anywhere in the target volume via a manipulator mechanism. In addition, light-emitting diodes are used for monitoring the detector stability. Various gamma sources are used for energy calibration: ^{208}Tl at 2.6 MeV, ^{16}N at 6 MeV, and 20 MeV photons from (p, t) reactions. A sonoluminescent source provides short pulses for time calibration, and a ^{8}Li source, produced by nuclear reaction, emits electrons with an energy spectrum which is directly related to the solar ^{8}B spectrum. This source can also be positioned with the manipulator mechanism.

Construction of the detector began in 1990 with the excavation works in the Sudbury mine. In 1997 the acrylic vessel was completed and the procedure of filling of the vessels started. Since summer 1999, SNO has been detecting solar neutrinos via the cc and es reactions. The preliminary cc spectrum published in June 2000 [130] shows agreement with the shape expected from the reference solar models; a thorough statistical analysis, however, has not yet been made available. The latter applies also to the integral ^{8}B ν_e-flux detected by SNO. Neutral-current detection will be accomplished in the second phase of the experiment, employing both of the methods described above. Then SNO alone—without referring to the results of the other solar neutrino experiments—can provide an answer to the question of whether oscillations take place for ^{8}B neutrinos in the energy region above 5 MeV, and, in addition, which types of oscillation occur—i.e. oscillations of ν_e to another flavour or to a sterile neutrino.

5. Implications

5.1. The solar neutrino puzzle

From the results of the running solar neutrino experiments, a number of conclusions can be drawn. Firstly, all solar neutrino experiments observe a statistically significant signal above zero. Hence, and this is a fundamental issue, the basic assumption of thermal nuclear fusion as the process of energy production in the Sun is proven to be correct.

Secondly, however, all solar neutrino experiments observe a significantly lower number of neutrinos than expected. This is illustrated in table 7 where the available experimental results

Table 7. The significance of the solar neutrino deficit as observed in six experiments. The quoted uncertainties are 1 σ, with statistical and systematic uncertainties quadratically summed. (This table is adapted and updated from [97]; as the reference solar model, that of [19] was used.)

	Home-stake	KAMIOKANDE	SUPER-KAMIOKANDE	GALLEX	GNO	SAGE
Experimental result Y_e	2.56 ± 0.22 (SNU)	2.82 ± 0.38 (10^6 cm^{-2} s^{-1})	2.42 ± 0.08 (10^6 cm^{-2} s^{-1})	$77.5^{+7.6}_{-7.8}$ (SNU)	$65.8^{+10.7}_{-10.2}$ (SNU)	$75.4^{+7.8}_{-7.4}$ (SNU)
				$74.1^{+6.7}_{-6.8}$ SNU		
Solar model prediction Y_t	$7.7^{+1.2}_{-1.0}$ (SNU)	$5.15^{+0.98}_{-0.72}$ (10^6 cm^{-2} s^{-1})	$5.15^{+0.98}_{-0.72}$ (10^6 cm^{-2} s^{-1})	129^{+8}_{-6} (SNU)	129^{+8}_{-6} (SNU)	129^{+8}_{-6} (SNU)
Deficit Y_e/Y_t	0.33 ± 0.06	$0.55^{+0.13}_{-0.11}$	$0.47^{+0.09}_{-0.07}$	0.60 ± 0.07	0.51 ± 0.09	0.58 ± 0.07
				$0.57^{+0.07}_{-0.06}$		
Significance of deficit	$5.0\,\sigma$	$2.9\,\sigma$	$3.8\,\sigma$	$5.3\,\sigma$	$5.2\,\sigma$	$5.4\,\sigma$
				$5.6\,\sigma$		

are shown and confronted with the respective theoretical expectations [19].

In calculating the significance of the observed deficit, one relies on estimations of theoretical uncertainties. It obviously must be ensured that the relevant physics processes in the solar interior as well as the input data like cross-sections and opacities are well understood. As discussed in section 3, the state-of-the-art reference solar models seem to provide the required reliable and experimentally tested description of the Sun.

5.2. Deficit of ^{8}B neutrinos

As long as the Homestake ^{37}Cl experiment was the only operative solar neutrino detector, the observed deficit was naturally assigned to a reduction in ^{8}B flux. As discussed in section 4, 76% of the expected signal stems from the highly temperature-dependent ^{8}B flux ($\phi(^8\mathrm{B}) \propto T^{18}$), and only 15% comes from the ^{7}Be neutrinos. Therefore, a reduction in the central temperature (which is an output parameter in the solar model computations) of $\approx$5%[12] could account for the Homestake result. In addition, other scenarios (e.g. modifying *ad hoc* the S_{17} cross-section) could be seen as responsible for the experimental result without violating the most fundamental constraints like that of the solar luminosity. For a review, see e.g. [35]. We note, however that any such attempt means using values different from those considered correct for one or more input parameters of the solar model computations. Moreover, these 'biased *ad hoc* modifications' have to be done in a correlated way in order to end up with the desired effect.

The situation changed with the availability of the KAMIOKANDE data in 1990, where about 50% of the ^{8}B flux was seen. For standard neutrinos (i.e. no neutrino masses, no neutrino oscillations) and assuming that the CNO and ^{7}Be flux predictions of the reference solar model are accurate, this implied an expectation of $\approx(4.8 \pm 0.7)$ SNU for Homestake, which is in conflict with the measured value of (2.56 ± 0.22) SNU. This conflict persists with the much more accurate SUPERKAMIOKANDE data which have meanwhile become available. Indeed, the SUPERKAMIOKANDE result implies a ^{8}B contribution to Homestake of about

[12] This can (in an *ad hoc* way) be achieved by putting in by hand certain input parameters in a correlated manner away from the values which are considered to be the correct ones.

3 SNU. This alone would still be compatible with Homestake results, taking into account the large uncertainty of the ^{8}B flux prediction. However, and this is a much more dramatic consequence, it implies (for massless standard neutrinos) the absence of any contribution of the medium-energy neutrino branches from the pp and CNO chains to the Homestake ^{37}Cl signal. In particular, no room is left for ^{7}Be neutrinos.

To resolve this problem also, it is no longer sufficient to 'just' lower the solar core temperature in order to reconcile the ^{8}B flux with the SUPERKAMIOKANDE measurement. As the intermediate-energy branches are much less sensitive to T_c than the ^{8}B flux, a temperature reduction can never accomplish a stronger reduction for the intermediate-energy neutrino branches than for the ^{8}B flux. In contrast, the requirement of an enhanced suppression of those intermediate-energy fluxes is a hint that neutrino oscillations are involved.

5.3. Deficit of ^{7}Be neutrinos—a hint of oscillations

The gallium experiments (GALLEX and SAGE) for the first time offered the possibility of covering the whole solar neutrino spectrum, including the most abundant pp branch. According to table 5, the expected neutrino signal is $Y_t = Y_{\mathrm{pp+pep}} + Y_{\mathrm{Be}} + Y_{\mathrm{CNO}} + Y_{\mathrm{B}}$, with $Y_{\mathrm{pp+pep}} = 73$, $Y_{\mathrm{Be}} = 34$, $Y_{\mathrm{CNO}} = 10$, and $Y_{\mathrm{B}} = 12$ (all values in SNU). From the SUPERKAMIOKANDE result one expects—in the case of standard neutrinos, i.e. the lack of any shape distortion of the ^{8}B-neutrino spectrum—a ^{8}B contribution of about 6 SNU. The solar model prediction for neutrinos from the CNO cycle is rather inaccurate, as it is for the ^{8}B flux; cf. sections 3 and 4. However, $Y_{\mathrm{pp+pep}}$ is almost model independent, as it is very strongly correlated with the solar luminosity. The ^{7}Be flux is only slightly model dependent, and even if we *ad hoc* set the CNO flux equal to zero in an arbitrary way, the expected minimal values for gallium experiments ($Y_t = (73 + 34 + 0 + 6) = 113$ SNU) are significantly higher than the actual observations of (74 ± 7) SNU for GALLEX/GNO and (75 ± 8) SNU for SAGE, respectively. As the measured values are still consistent with the expected pp flux, it is likely that the ^{7}Be neutrinos can be considered as 'missing'. This deficit cannot be explained by applying minor modifications to the solar models, as illustrated in figure 9.

This puzzle of missing ^{7}Be neutrinos can even be shown in a maximally conservative calculation which is completely independent of any solar model details [7]. In contrast, a constraint for the ^{7}Be flux is determined from the single requirement that the following experimentally determined parameters are reconciled: the solar luminosity, and the SUPERKAMIOKANDE and the GALLEX/GNO results. The branching ratios between the pp-I, pp-II, and pp-III cycles are treated as free parameters. Figure 10 shows the 90% c.l. region, indicating again a severe depression of the ^{7}Be-neutrino flux.

If, on the other hand, pp rather than ^{7}Be neutrinos were responsible for the deficit observed in the gallium experiments, it would be impossible to reconcile this with the solar luminosity without invoking non-standard neutrino properties.

In summary, we conclude that standard model (i.e. massless) neutrinos, which the results of the calculations as shown in figures 9 and 10 are based on, obviously cannot reasonably describe the experimental results. The latter, in contrast, provide strong evidence that the flavour content of solar neutrinos is changed on their way from the interior of the Sun to the Earth.

5.4. Neutrino oscillation scenarios

Trying to reconcile the experimental results with neutrino oscillations between two flavours, four-parameter regions in the Δm^2–$\sin^2 2\theta$ plane turn out to provide a reasonably good fit to

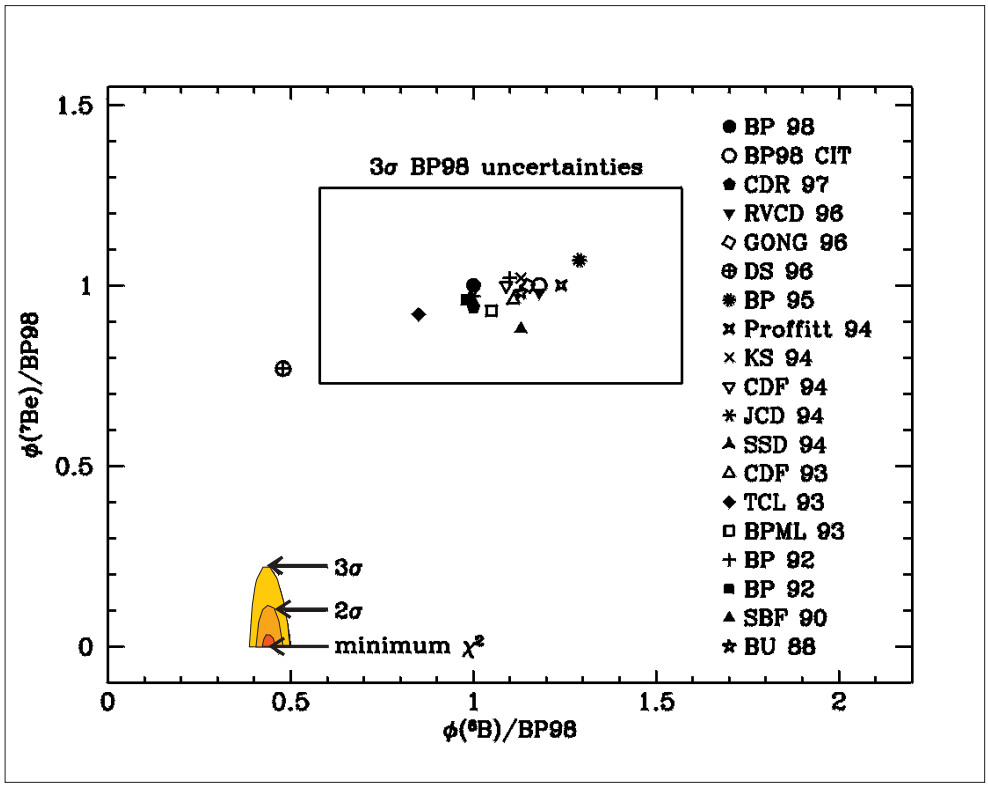

Figure 9. Predicted fluxes for the ^{7}Be- and ^{8}B-neutrino branches from several solar model computations [22]. The area allowed from a combined fit to the results of Homestake, (SUPER-) KAMIOKANDE, GALLEX and SAGE—assuming massless standard neutrinos—is also indicated. With the best-fit value lying in the unphysical region $\phi_{\mathrm{Be}} < 0$, even the three-sigma contour is far away from the model predictions.

the data. They are schematically depicted in figure 11.

One of them describes neutrino oscillations in the vacuum between the Sun and the Earth, with Δm^2 in the region of 10^{-10} eV^2 and essentially maximal mixing, $\sin^2 2\theta \simeq 1$.

The remaining three scenarios rely on resonant amplification of oscillations inside the Sun via the MSW effect (cf. section 2). Though the exact locations of the best-fit parameter sets in the Δm^2–$\sin^2 2\theta$ plane depend on the reference solar model being referred to[13] [27], three regions can be located. One of them is located around $\Delta m^2 \approx 10^{-5}$ eV^2 and mixing angles in the range $10^{-3} \lesssim \sin^2 2\theta \lesssim 10^{-2}$. For this area of allowed parameters, the mass range is insensitive to, but the mixing angle depends on, the ^{8}B flux prediction of the reference solar model. This region is generally referred to as the 'small-mixing-angle solution' (the SMA solution), in contrast to the second allowed region around $10^{-5} \lesssim \Delta m^2\ \mathrm{eV}^{-2} \lesssim 10^{-4}$ and almost maximal mixing, which is, accordingly, called the 'large-mixing-angle solution' (the LMA solution). At a low confidence level, a third region around $\Delta m^2 \approx 10^{-7}$ eV^2 and essentially maximal mixing appears for one of the reference solar models [21] (the LOW solution).

[13] The main reason is that, due to the present uncertainties of solar modelling, the various reference model computations yield somewhat different predictions for the ^{8}B-neutrino flux $\Phi(^{8}\mathrm{B})$ (cf. section 3).

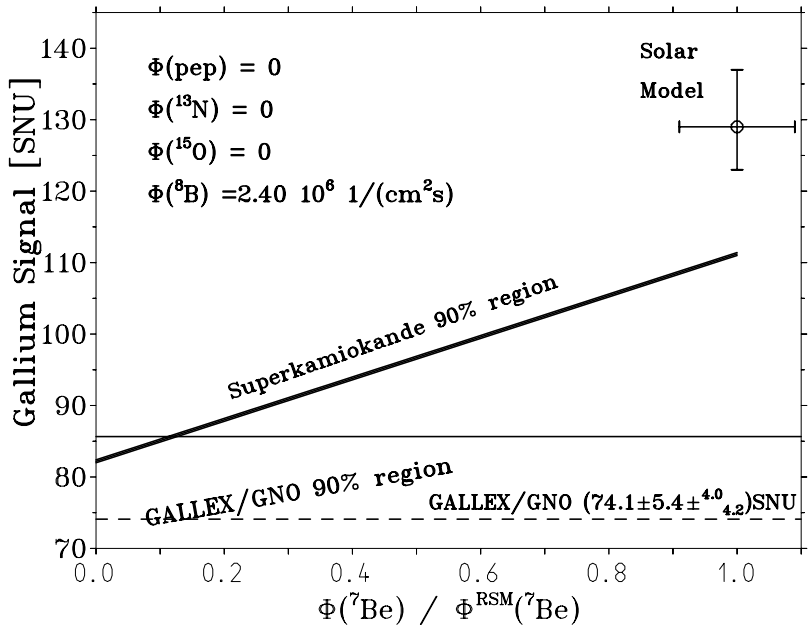

Figure 10. The conservative experimental constraint for the solar ^{7}Be flux, obtained in a calculation independent of any solar model details. The branching ratios between pp-I, pp-II, and pp-III are treated as free parameters, with only the solar luminosity serving as a boundary condition. In the case of no neutrino oscillations (i.e. for massless neutrinos), the results from the SUPERKAMIOKANDE and GALLEX/GNO experiments suffice to severely constrain the ^{7}Be flux—even for the entire absence of CNO and pep neutrinos.

Recently, several analyses with mixing among all three neutrino flavours have been published. For the information which is available from the experiments, however, they do not, for the time being, yield any in principle new neutrino parameter regions. We therefore do not yet face the necessity of shelving *ad acta* the easy-to-interpret two-neutrino oscillation scenario.

5.5. A way to pinpoint neutrino parameters—solar neutrino spectroscopy

Which of the neutrino oscillation scenarios compatible with the experimental data is in fact realized in Nature is still to be investigated. However, there is a realistic potential for achieving this goal by exploiting the various pronounced features which are expected for the different allowed regions in the Δm^2–$\sin^2 2\theta$ plane.

For the vacuum oscillation solution with neutrino-mass-squared differences in the $\Delta m^2 \approx 10^{-10}$ eV^2 range, the oscillation length for neutrino energies around 1 MeV is comparable to the seasonal distance variation caused by the eccentricity of the Earth's orbit. Therefore, in particular for monoenergetic neutrino lines like the ^{7}Be or pep branches, a pronounced seasonal signature can be detected. In section 6.1 we will discuss this issue in detail in the context of the upcoming BOREXINO project, which is perfectly suited to settling the question. We therefore mention at this point only that the operating experiments GNO and SAGE, with augmented statistical accuracy, also have a good chance of detecting the predicted seasonal variations, thanks to the large ^{7}Be contribution in their spectral sensitivity (cf. table 5) [73, 142]. The real-time capabilities of these radiochemical experiments with a realized time resolution of

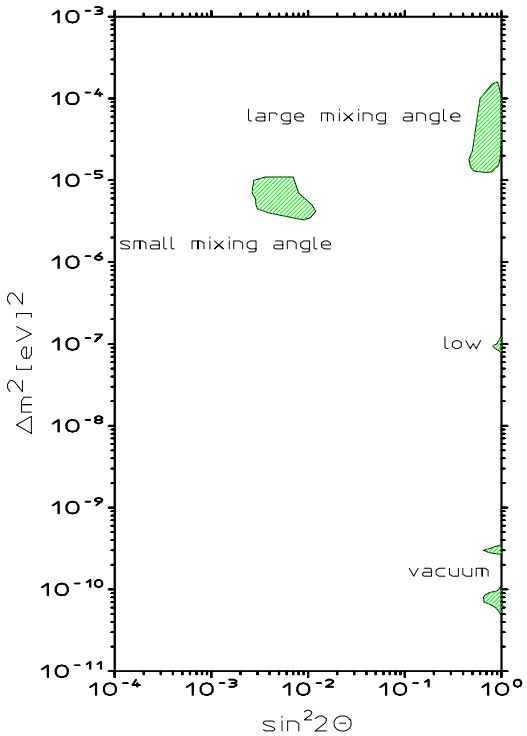

Figure 11. Allowed parameter regions (95% c.l.) for solar neutrino oscillations after analysis of the measured fluxes in the gallium, chlorine, and SUPERKAMIOKANDE experiments. Information from the spectral shape of the ^{8}B measurement and the day–night analysis of SUPERKAMIOKANDE is not taken into account. The latter disfavours the 'small-mixing' and 'vacuum' solution at 95% c.l., as well as oscillations into sterile neutrinos.

some weeks[14] are perfectly sufficient for this kind of study, which investigates rate changes on a several-month scale.

Matter-enhanced neutrino flavour conversions also exhibit pronounced signatures which are characteristic for the different areas in the Δm^2–$\sin^2 2\theta$ plane. Both the SMA and the LMA solutions predict an energy-dependent distortion of the spectral shape in the energy range accessible to the operating experiments. In the LMA case, the distortion affects essentially all neutrino branches, in particular also the low-energy pp neutrinos. For the ^{8}B neutrinos in the energy range above $\approx$5 MeV, which can be tested by SUPERKAMIOKANDE, however, the LMA-predicted suppression is almost constant with energy. This means that the experiment should observe a global ν_e-flux reduction but not detect a substantial spectral distortion with respect to the shape expected for standard model neutrinos. The recent SUPERKAMIOKANDE data from a 1117 d data sample support this feature [135].

In contrast to the LMA region, the SMA solution exhibits a more pronounced spectral distortion in the energy range of some MeV. For neutrino parameters lying in the SMA region, the no-oscillation probability shows a characteristic 'bathtub'-like shape. Whereas pp neutrinos and the 384 keV ^{7}Be line remain essentially unaffected, in particular the medium-energy region around 1 MeV, i.e. the pep and the 862 keV ^{7}Be line, is almost completely

[14] The minimal achievable time resolutions were, due to the minimal time needed for performing the extraction of germanium from the target, $\approx$1 d.

suppressed. Towards higher energies, the oscillation probability decreases again, therefore leading to a substantial shape distortion of the low-energy part of the ^{8}B-neutrino spectrum. For SUPERKAMIOKANDE this means that the low-energy bins should be more strongly suppressed than the high-energy bins. We note, as a word of caution, that whether or not a SMA parameter set leads to an energy-dependent spectral distortion which is observable in the SUPERKAMIOKANDE low-energy bins depends to some extent on details of the solar model referred to, particularly on the S_{17} cross-section value. As discussed in section 3, S_{17} is not accurately determined experimentally. However, direct measurement of the ν_e-components of the medium-energy neutrino branches around 1 MeV will confirm or definitely rule out the SMA solution without suffering from model uncertainties.

Both the LMA and SMA regions predict a partial regeneration of the ^{8}B-electron-neutrino component by an MSW-like resonant amplification of the oscillation, probability in the matter of the Earth. Therefore, SUPERKAMIOKANDE might see a flux enhancement during the night, when neutrinos traverse the Earth's interior. Whereas for neutrino parameters in the SMA region and neutrino energies exceeding the SUPERKAMIOKANDE energy threshold, the resonance condition is only fulfilled when neutrinos traverse the Earth's inner core, the LMA region predicts an enhancement throughout more or less the entire night. As already discussed in section 4.4, SUPERKAMIOKANDE reported a slight—though statistically not yet significant—day–night asymmetry, which tends to favour the LMA interpretation.

For the LOW region, a pronounced day–night effect is predicted for the medium-energy neutrinos around and below 1 MeV. Unfortunately, the time resolution of the radiochemical gallium experiments is not sufficient for directly testing for this effect, and the statistical accuracy that they have reached so far is not sufficient to allow one to indirectly probe it by investigating the data for the presence of an ≈5 SNU [55] difference between winter and summer data, caused by the inclination of the Earth. Therefore, the results of the upcoming experiments BOREXINO and KAMLAND, which directly investigate the medium-energy region, must be awaited.

6. Prospects: future solar neutrino experiments

6.1. BOREXINO

The aim of BOREXINO, placed in the Italian Gran Sasso Underground Laboratory, is the first individual determination of the solar ^{7}Be-neutrino flux [31]. Neutrinos will be detected by elastic scattering on electrons of a liquid organic scintillator with a total mass of about 300 tons, $\nu + e^- \rightarrow \nu + e^-$. This scattering process is described in standard electroweak theory, including radiative corrections, at an accuracy of ≈3% for the energy range of ≈1 MeV and below. The monoenergetic ^{7}Be neutrinos with $E_\nu = 0.862$ MeV yield a unique flat-box recoil profile with a spectral edge at 0.66 MeV. The edge is determined by the energy of the monochromatic ^{7}Be-neutrino branch; thus it offers a signature for the reaction.

Figure 12 shows schematically the detector design of BOREXINO.

A fiducial volume of about 100 t for solar neutrino interaction can be defined, and the outer part of the scintillator sphere serves as an active additional shielding against external background. Between the two steel tanks, deionized water acts as shielding against external gamma and neutron radiation and in addition as a medium for an outer Cherenkov detector in order to recognize high-energy intersecting cosmic muons.

6.1.1. Neutrino rates in BOREXINO. The scattering of ν_e is driven by the charged (cc) and neutral (nc) weak currents, i.e. $W^\pm$ and Z^0 exchange, whereas ν_μ- and ν_τ-scatterings occur

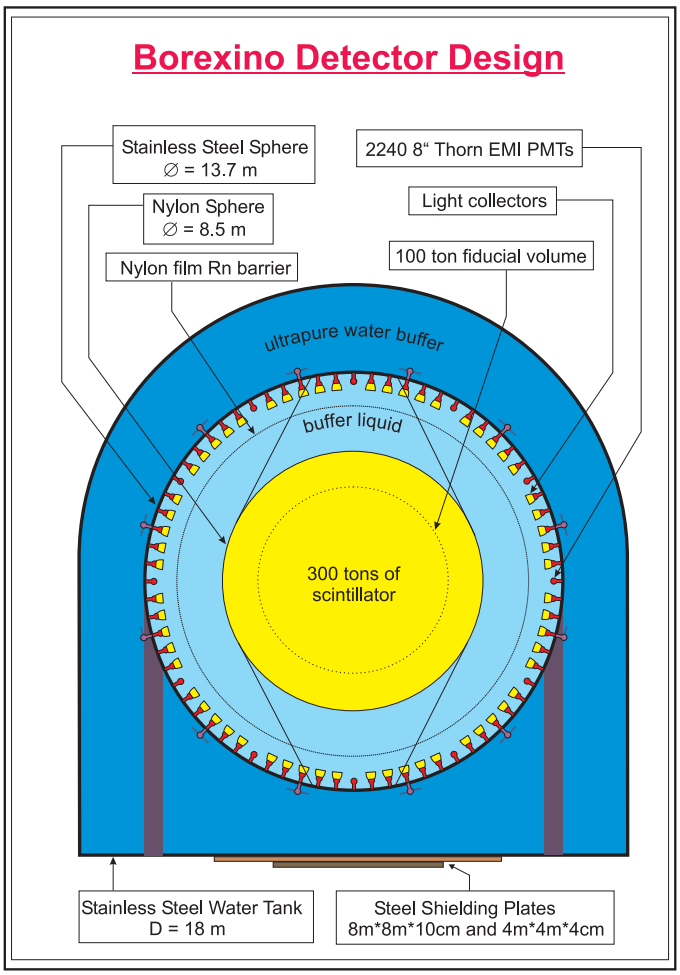

Figure 12. A schematic sketch of BOREXINO. The ultrapure scintillator (300 t) inside a nylon vessel is shielded differentially by means of a liquid buffer (1040 t), a steel sphere 13.5 m in diameter on which the 2200 photomultiplier tubes are mounted, and an outer water buffer which is contained in an external steel tank with dimensions of 18 m. A transparent nylon shroud hinders radon convection in the liquid-buffer region. Additional tubes mounted on the outer surface of the steel sphere allow detection of penetrating muons via the Cherenkov light that they emit when traversing the outer water buffer.

only via the nc reaction. Thus the effective cross-section depends on the neutrino flavour. In the ^{7}Be-neutrino signal window, the counting rate which is exclusively due to nc reaction is 23% of the total ν_e–e^- scattering rate. Thus, even for complete conversion of the ^{7}Be neutrino into another flavour, BOREXINO will record a significant 23% of the solar model signal.

Sterile neutrinos. The ^{7}Be neutrino signal will be less than this limit if neutrinos are converted to sterile, e.g. right-handed species, because in this case the interaction is reduced to vanishing levels by the factor $(m_\nu/E_\nu)^2$. Barring an unlikely mechanism that severely reduces only the ^{7}Be flux without affecting basic features of the reference solar model and helioseismology results [139], BOREXINO offers a unique method for clear recognition of sterile neutrinos.

MSW-converted neutrinos. Both the SMA scenario and the LMA solution result only in ^{7}Be ν_e-flux deficits (cf. section 5), whereas the integral ^{7}Be-neutrino flux in all three flavours ($\nu_e+\nu_\mu+\nu_\tau$) remains unaffected. However, the sizes of the ν_e-deficits differ substantially in the two cases. For the SMA region, the ^{7}Be ν_e are almost completely converted. Thus, we expect a pure $\nu_{\mu,\tau}$-signal in BOREXINO, i.e. close to the limit of $\approx$0.23 of the solar model prediction. In the LMA region, the conversion is less strong, $\approx$47% of the solar model flux [19]. Hence the expected signal in BOREXINO is $\approx$0.6 of the solar model prediction.

For the LOW region, the time-averaged signal in BOREXINO is about the same as in the LMA area, but the ^{7}Be-neutrino signal shows a remarkable day–night variation [31]. At night, solar neutrinos reach the detector after passage through the Earth, where some of the $\nu_{\mu,\tau}$ from conversion in solar matter can be reconverted to ν_e by terrestrial matter, thus increasing the signal in BOREXINO. As the day–night signal difference depends on the angle of the incident neutrino, a slight seasonal variation should in addition be expected.

Vacuum oscillations. Due to the Earth's eccentric orbit, neutrino vacuum oscillations would result in significant seasonal fluctuations of the counting rate of BOREXINO for $\Delta m^2 \approx 10^{-10}$ eV^2. Figure 13 shows the predictions for two values of Δm^2, both compatible with present data.

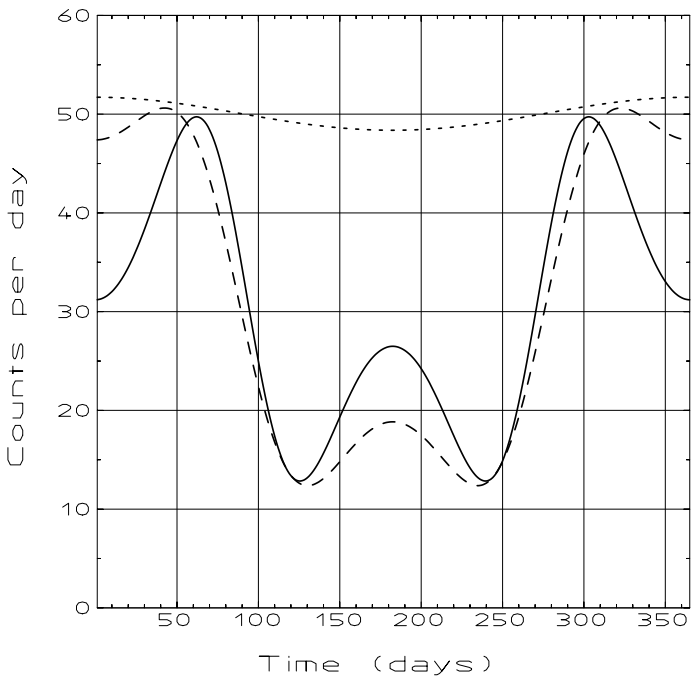

Figure 13. The seasonal variation of the counting rate in BOREXINO in the case of vacuum oscillations. The dotted curve refers to the expected signal in the no-oscillation case, its depletion in summer indicating the Earth's eccentricity which accounts for an $\approx$7% effect. Neutrino oscillations appear in a very distinct manner for the monoenergetic ^{7}Be line. Two oscillation parameter sets, $\Delta m^2 = 4.2 \times 10^{-10}$ eV^2 (full line) and $\Delta m^2 = 3.2 \times 10^{-10}$ eV^2 (dashed), have been used to demonstrate that this parameter can be determined with high accuracy. In both cases, full mixing was assumed. The broadening of the Be line due to the temperature in the solar centre as well as the source position distribution in the Sun have been taken into account.

As Δm^2 becomes larger, the time variations become faster, approaching weekly and daily oscillations. Such values of Δm^2 are allowed for the ^{7}Be line only up to $\Delta m^2 \approx 10^{-8}$ eV^2, when the oscillations become so fast as to lose coherence [132].

Table 8 summarizes the expected neutrino rates in BOREXINO depending on the physics scenario. Here not only solar ^{7}Be-neutrino fluxes, but also the numbers of pep, ^{8}B, and CNO neutrinos are shown. The latter is calculated for the energy range below 5.5 MeV which might not be covered by Cherenkov detectors like SNO and SUPERKAMIOKANDE. All interaction rates are calculated at tree level; radiative corrections are not included.

Table 8. Counting rates (events per day) expected in BOREXINO via ν–e$^-$ scattering for four physics scenarios: the reference solar model (RSM) [19], and the three MSW scenarios LMA, SMA, and LOW (cf. section 5). The rates are calculated for the mean Sun–Earth distance, for 113 m^3 fiducial volume, and for a pseudocumene scintillator target. No radiative corrections are included. For the LMA and SMA solution, $\Delta m^2 = 1.8 \times 10^{-5}$ eV^2, $\sin^2 2\theta = 0.76$ and $\Delta m^2 = 5.4 \times 10^{-6}$ eV^2, $\sin^2 2\theta = 5.5 \times 10^{-3}$ have been used, respectively. The parameters utilized for the LOW scenario are $\Delta m^2 = 7.9 \times 10^{-8}$ eV^2, $\sin^2 2\theta = 0.96$.

Recoil energy window (MeV)	Neutrino branch	RSM (d^{-1})	LMA (d^{-1})	SMA (d^{-1})	LOW (d^{-1})
0.25–0.80	pp	0.22	0.15	0.08	0.13
	^{7}Be	43.3	24.4	9.20	22.8
	pep	2.0	0.95	0.39	1.03
	^{13}N	4.0	2.27	0.87	2.13
	^{15}O	5.5	2.86	1.12	2.86
	^{17}F	0.07	0.03	0.01	0.03
	^{8}B	0.08	0.03	0.04	0.04
	Integral	55.2	30.7	11.7	29.0
0.80–1.50	pep	1.43	0.68	0.28	0.73
	^{13}N	0.13	0.07	0.03	0.07
	^{15}O	1.80	0.86	0.35	0.92
	^{17}F	0.02	0.01	0.00	0.01
	^{8}B	0.10	0.04	0.05	0.05
	Integral	3.48	1.66	0.71	1.78
1.50–5.50	^{8}B	0.454	0.174	0.217	0.232

6.1.2. Background in BOREXINO. The energy-dispersive observation of such rare low-energy events has never been attempted because of the formidable intrinsic background of the detector medium itself, arising from ubiquitous natural radioactive contaminants. As discussed in section 4, the only energy-dispersive observations of solar neutrinos to date have therefore been made above ≈5 MeV.

The radioactive contaminants of most concern in BOREXINO are the primordials ^{40}K, ^{238}U and ^{232}Th with their decay products ^{226}Ra and ^{210}Pb, the noble gases ^{222}Rn and ^{85}Kr, and ^{14}C which obviously cannot be removed chemically from an organic liquid. The demands on purity in terms of radioactivity in BOREXINO, especially for the scintillator itself, are challenging. In order to be able to extract a clear signal over background also in the case of

total flavour conversion, an intrinsic concentration in uranium and thorium of about 10^{-16} g g^{-1} should not be significantly exceeded, and the ratio $^{14}C/^{12}C$ is tolerable to an upper limit of $\approx 10^{-18}$.

Active background recognition '*in situ*' is based on identification of alpha pulses from the uranium and thorium decay chains by means of pulse shape information, identification of Bi–Po delayed coincidences, and identification of the ^{220}Rn–^{216}Po delayed alpha–alpha coincidence sequence. The former is used to determine the radium concentration; the latter provides a measure of the thorium contamination in the scintillator. The content in uranium itself can be determined by analysing scintillator samples with the neutron activation analysis (NAA) method. Cosmogenically produced radioactive nuclei can be tagged by the muon veto system (see figure 12).

In order to test the feasibility in principle of BOREXINO, the collaboration was running the Counting Test Facility CTF at the Gran Sasso Underground Laboratory. The results obtained were encouraging: $^{14}C/^{12}C$: 1.94×10^{-18}; ^{238}U: $(3.5 \pm 1.3) \times 10^{-16}$; ^{232}Th: $(4.4 \pm 1.5) \times 10^{-16}$. A complete discussion of the CTF results including experimental techniques for further background suppression are given in [45] and [46]. In addition, highly sensitive NAA has been developed, providing an independent test of the radiopurity which allows important tests on the secular equilibrium of the decay chains. With NAA, an upper limit for uranium in organic liquid scintillators of $^{238}U < 1 \times 10^{-17}$ (90% c.l.) has been measured after several purification steps based on silica-gel chromatography and water extraction. By this method, concentration values or limits have been determined for various isotopes, including synthetic nuclei, for different detector materials [89].

6.2. KAMLAND

The KAMLAND project [134] started in 1997, aiming for a long-baseline reactor neutrino measurement in order to probe the LMA MSW scenario. The primary target of KAMLAND (Kamioka liquid scintillator antineutrino detector) is the direct search for neutrino oscillations using electron antineutrinos ($\bar{\nu}_e$) from nuclear power reactors at distances between 140 km and 210 km. Neutrino detection employs the inverse beta decay on free protons of the scintillator: $\bar{\nu}_e + p \rightarrow e^+ + n$ at an energy threshold of 1.8 MeV. Signal separation from background events is possible via the delayed coincidence between the prompt e^+ and the delayed 2.2 MeV γ arising from neutron capture on a proton. In measuring the positron energy, neutrino spectroscopy is possible, because of the negligible kinetic recoil energy of the neutron.

Using reactor neutrinos, neutrino oscillations can be observed only in the disappearance mode, since the energies of the reactor $\bar{\nu}_e$ are limited to $\approx$9 MeV. However, the expected neutrino mixing in the LMA region is large and the effect is therefore observable even in a disappearance experiment. Since the distance between the neutrino source and the detector is long enough, the corresponding L/E_ν parameter region of the LMA scenario can be probed[15]. The detector assembly is basically equivalent to that of BOREXINO. However, the detector volume is significantly larger. About 450 inverse beta events are expected in the no-oscillation case for a fiducial mass of 600 t. This is to be compared to the expected background rate of time-correlated signals, which should be $\approx$8 per year assuming 10^{-14} g g^{-1} for U and Th, 10^{-12} g g^{-1} for K, and 0.5 mBq m^{-3} for Rn concentrations in the scintillator.

In a second phase, the collaboration plans to aim for observation of ^7Be and ^8B solar neutrinos. With neutrino scattering on electrons, the same reaction as in BOREXINO is going to be used. The photoelectron yield of the detector set-up is $\approx$110 per MeV energy release, i.e. only about 27% of that of BOREXINO. However, it is good enough to reach a threshold

[15] As antineutrinos are being investigated, this conclusion holds under the assumption of CPT conservation.

of ≈300 keV for the recoil electron and to be sensitive to ^{7}Be neutrinos. About 940 ^{8}B events per year and 110 ^{7}Be signals are expected according to the solar model prediction for 560 t and 300 t fiducial mass, respectively.

Since the detection reaction is the same as in BOREXINO, the two experiments have similar potentials for distinguishing between different physical scenarios, and we refer the reader to the discussion in the previous section. In situations where the statistics is crucial, KAMLAND could offer a conclusive result. An example is the detection of ^{8}B neutrinos in the energy range below the threshold of SUPERKAMIOKANDE and SNO, where the counting rate in BOREXINO is expected to be rather small (i.e. ≈0.2 counts per day for the MSW regimes; cf. table 8), which makes the study of the spectral shape awkward. However, the cosmic muon flux being ≈9 times higher compared to that of Gran Sasso, there is a caveat: the cosmogenic background in KAMLAND is substantially higher and might turn out to constitute a serious problem.

It should be noted that the LMA scenario will also be probed via long-baseline measurement using European reactors in BOREXINO, however at a much smaller counting rate of ≈30 events per year [129]. With the scintillator purity achieved in the CTF and due to the good shielding against cosmic muons, the background rate in BOREXINO is expected to be significantly below one event per year.

Both experiments, KAMLAND and BOREXINO, are aiming for detection of terrestrial neutrinos, too. Hence, the radiogenic heat of the Earth which stems mainly from U and Th decays can be measured for the first time. The expected flux depends strongly on geophysical models of the abundance of U and Th in the continental crust, oceanic crust, upper mantle, and lower mantle. Due to the different locations of the two experiments, the comparison of results on terrestrial neutrinos in KAMLAND and BOREXINO can distinguish between these models. For details, see e.g. [119].

6.3. GNO upgrade: GNO-66 and GNO-100

The Gallium Neutrino Observatory at Gran Sasso currently employs the GALLEX target of 30 tons of gallium in the form of 101 t of $GaCl_3$ solution. However, to fully exploit the potential of performing a high-precision determination of the integral solar neutrino flux in the cc mode, and, in particular, to exploit the real-time capabilities of the experiment for investigating potential time variations, a substantial improvement of the statistical significance for both the overall data set and individual extractions is mandatory.

Apart from improving on the systematic error, the collaboration plans to increase the target mass to 66 tons and, in a further step, to 100 tons [71]. With a target mass of 100 tons, corresponding to a neutrino capture rate of as much as about three events per day, the experiment allows one to even probe time variations on the month scale, as e.g. expected for the vacuum oscillation scenario described in section 5. Figure 14 shows the estimated evolution of the statistical and systematic error of the overall GNO result. The ultimate goal is to reach an accuracy of better than 4% for the combined overall result.

To underline the potential offered by this precision, we note that for a neutrino capture rate of 74 SNU, i.e. the final GALLEX number properly combined with the additional data from the first 19 GNO runs, an error that small would allow one to exclude standard model neutrinos by just considering the solar luminosity[16]— without reference to any solar model or any other solar neutrino experiment!

[16] The minimum requirement for preserving the observed solar luminosity is 80 SNU. This most conservative number, the lowest which is allowed for standard neutrinos, does not require any neutrinos of higher energy than those from the initiating pp reaction to be produced in the solar core.

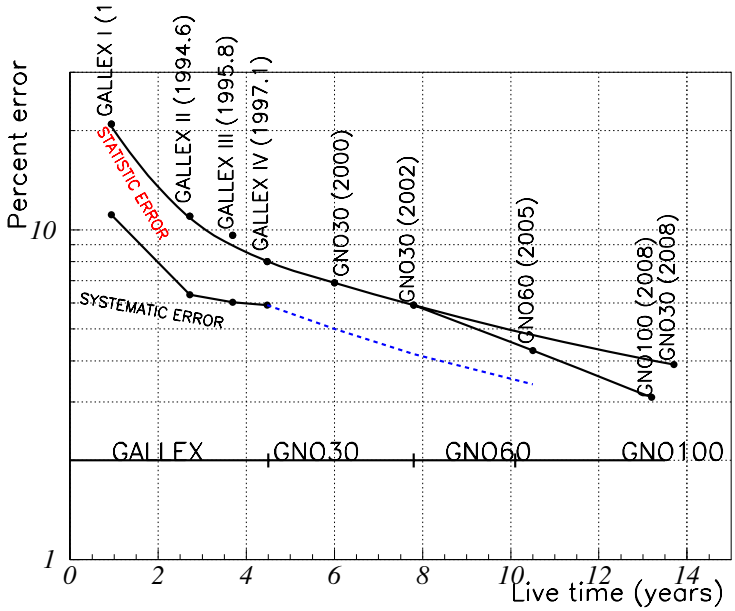

Figure 14. Estimated error evolution for GNO [71]. The first milestone (GNO30-2000) has been accomplished [73].

The first step, the upgrade to 66 tons, can be accommodated without major constructional endeavour within the existing experimental installations of GNO. For a further upgrade to 100 tons, some enlargements of the storage and extraction apparatus must be foreseen.

In addition to increasing the mass of the target isotope, the GNO collaboration is investigating the feasibility of employing cryogenic detectors instead of proportional counters for the detection of the ^{71}Ge back-decay [9, 10]. Apart from gaining in systematic error, the main motivation for this 'R&D' which has shown promising progress [102, 143] is the desire to increase the counting efficiency by about 30–35% to a value close to 100%. Improving this number, which directly influences the statistical uncertainty, is equivalent to a corresponding increase of the target mass. There is some prospect, therefore, that the GNO performance might even exceed the expectations outlined in the proposal [71] and shown in figure 14.

6.4. The day–night effect in the Homestake iodine experiment

In the Homestake gold mine, the location of the chlorine experiment, a second radiochemical solar neutrino detector is being installed [40]. It will initially have a target mass of 100 tons of ^{127}I as NaI dissolved in water (altogether 230 tons of solution). First test runs were started in 1997.

^{127}I is an appropriate target material for the charged-current-mode investigation of solar neutrinos of intermediate energy, in particular ^{7}Be neutrinos. As the transition to the ^{127}Xe ground state is forbidden by angular momentum conservation, the lowest nuclear state accessible in the reaction $^{127}\mathrm{I} + \nu_e \rightarrow {}^{127}\mathrm{Xe} + \mathrm{e}^-$ is an $I = 3/2^+$ level 125 keV above the ^{127}Xe ground state, resulting in an energy threshold of 789 keV, well below the 860 keV ^{7}Be-neutrino line. As, in contrast to the case for ^{37}Cl, there is no enhanced contribution from an isobaric analogue state, the spectral response of the ^{127}I detector is to some extent complementary to the Homestake ^{37}Cl experiment.

Though detailed differential cross-section measurements remain to be done, from theoretical considerations, the ratio of the cross-section of 1 MeV neutrinos to that in the ^{8}B energy domain is expected to be about four times higher than for ^{37}Cl [52, 53, 87]. Therefore, the experiment will provide valuable information on the contribution of ^{7}Be neutrinos in the cc mode.

The technique of the ^{127}I experiment is radiochemical, with an extremely short extraction time constant of only 12 min (corresponding to 99% Xe recovery in one hour of operation) [40]. Therefore, the experiment exhibits real-time capabilities which allow one to perform two extractions per day, one at 6 a.m. to acquire the xenon produced at night, and the other at 6 p.m. to extract the ^{127}Xe produced during the day. The day and the night samples are accumulated in two separate charcoal traps for a period of about a month, before being transferred to proportional counters in order to detect the back-decay of ^{127}Xe ($T_{1/2} = 36.4$ d). ^{127}Xe detection is virtually background free, due to the distinctive signature of an Auger electron–γ coincidence.

The comparison of the results for the day and night samples allows one to probe matter-enhanced neutrino conversion taking place in the Earth (the terrestrial MSW effect). This information will be complementary to tests of the day–night effect performed by SUPER-KAMIOKANDE, due to the sensitivity of the ^{127}I experiment to ^{7}Be neutrinos.

6.5. The far future

6.5.1. LENS. The proposed LENS (Low Energy Neutrino Spectroscopy) project [107] aims for low-energy solar neutrino spectroscopy in the cc mode. Here inverse beta decay on nuclei with small energy thresholds is going to be used. Since electron scattering as it is used in BOREXINO is sensitive to both charged- and neutral-current interaction, flavour conversion can be proven by comparing the LENS and BOREXINO event rates. For the SMA MSW scenario, LENS will see a drastically reduced flux, whereas BOREXINO and KAMLAND will measure the flavour-converted part with an amplitude of $\approx$23%, according to the reference solar model. In the case of conversion into sterile neutrinos, all three experiments would measure a ^{7}Be flux which is consistent with zero. Vacuum oscillations provide seasonal variations in the cc measurement of ^{7}Be neutrinos in LENS. However, because of the substantially higher statistics in BOREXINO and KAMLAND, the latter experiments are much better suited for providing clear evidence for vacuum oscillations.

For LENS, several target nuclei have been considered. Among them, ^{160}Gd and ^{176}Yb are being favoured by the collaboration. Both offer energy thresholds low enough to enable pp-neutrino detection. Due to the isomeric states occupied in the daughter nuclei, delayed coincidence techniques can be applied to achieve a substantial background suppression. Since the target nuclei will be embedded inside an active detection material (e.g. liquid scintillator), neutrino spectroscopy is possible. Transition strengths have been calculated [118] and are confirmed experimentally by measuring the nuclear matrix elements via (p, n) and (^{3}He, ^{3}H) reactions [43], however only with an accuracy of 20–30%. For reasonable counting rates, target masses of the order of $\approx$10 t are required. Due to the large uncertainty in the cross-section, direct calibration with a synthetic neutrino source of known activity (e.g. ^{51}Cr), as was performed in the gallium experiments GALLEX and SAGE [1, 62, 65], is mandatory.

Table 9 lists some characteristic features of both target isotopes which were investigated for LENS. It is evident that the very low energy release ($\approx$100 keV) of the delayed event and the short coincidence time require a sensitive and fast detection concept. Since not only the time correlation but also the position correlation between prompt and delayed events should be used as a neutrino signature, the detector has to be position sensitive as well. The collaboration

Table 9. Potential reactions for a LENS-type neutrino experiment employing the charged-current mode. In principle, the energy threshold $E_{\rm thr}$ allows neutrino spectroscopy of all solar neutrino branches. Delayed coincidence techniques can be applied to improve background suppression. The table lists the counting rate for solar pp, Be, and pep neutrinos per ton of target (in natural isotopic abundance) and per year.

	$\nu_e(^{160}\mathrm{Gd}, ^{160}\mathrm{Tb})e^-$	$\nu_e(^{176}\mathrm{Yb}, ^{176}\mathrm{Lu})e^-$
$E_{\rm thr}$	244 keV	301 keV
$E_{\rm delayed}$	138.7 keV	72 keV
$\tau_{\rm delay}$	8 ns + 87 ns	50 ns
Isotopic abundance	21.8%	12.8%
pp rate	10 a^{-1} t^{-1}	21.7 a^{-1} t^{-1}
^{7}Be rate	7.5 a^{-1} t^{-1}	13.1 a^{-1} t^{-1}
pep rate	0.5 a^{-1} t^{-1}	0.83 a^{-1} t^{-1}

is testing liquid scintillators loaded with Gd and Yb at the ≈10% concentration level—with encouraging first results [120]. However, it remains to be demonstrated that such a heavily doped scintillator, exhibiting long-term chemical stability, a high enough light output and transparency, and a sufficiently low intrinsic activity, can be manufactured in the required quantities.

Fake neutrino candidates can arise from random coincidences, where the dominant background for the delayed event comes from ^{14}C beta decays in the organic solvent. The prompt signal can be mimicked by primordial radioactive isotopes (see the background discussion for BOREXINO in section 6.1) and contaminants endemic to rare earths (e.g. Gd, Sm, Lu). Random coincidences can be measured *in vivo* and removed statistically from the signal spectrum.

However, this is not possible for *correlated* background events. These can arise mainly from ^{231}Th, a daughter of ^{235}U, whose decay scheme mimics the neutrino signal. The production of Yb or Gd therefore should achieve a purity in U at a level of 10^{-15}, and for the solvent itself this value should reach 10^{-16}, as was obtained for BOREXINO for a pure scintillator without Gd or Yb loading. Cosmogenically created cascades have been found in Gd, where ^{151}Gd, ^{153}Gd, and especially ^{159}Eu are produced in hadronic showers from highly energetic muons. No cosmogenic background candidate has been identified for Yb.

The LENS collaboration submitted a letter of intent to the scientific committee of the Gran Sasso Laboratory in spring 1999. A proposal is in preparation.

6.5.2. Radiochemical lithium detector. A radiochemical experiment employing the reaction $^7\mathrm{Li} + \nu_e \rightarrow ^7\mathrm{Be} + e^-$ (energy threshold 0.86 MeV) can add to the information on the medium-energy part of the solar ν_e-spectrum extracted from the ^{37}Cl and future ^{127}I experiments. It should be noted, however, that the spectral response for the lithium capture reaction is not dominated by one particular spectral component—as is the iodine reaction—but is instead unspecific. ^{7}Be decays with a half-life of 53 d by electron capture. However, as only 10% of the decays populate a 478 keV excited nuclear level, the detection of the 55 eV Auger electron from orbital shell de-excitation and the 57 eV nuclear recoil is mandatory for a future Li detector. An Italian–Russian collaboration is studying the feasibility of a ten-ton detector, where cryogenic microcalorimeters will be employed for lithium detection [57, 98]. First results on both the chemical procedure for handling the target and extracting the beryllium and the low-temperature counting technique are promising.

6.5.3. HERON. The HERON project aims at an energy-dispersive real-time measurement of primarily pp and ^{7}Be neutrinos [4, 23, 106]. It is planned to employ a 10 t target of superfluid ^{4}He and to rely on an entirely new particle detection concept.

Recoil electrons from neutrino–electron scattering in the superfluid ^{4}He will produce both rotons and ultraviolet photons at an extraordinarily high multiplicity: about 10^7 rotons/phonons and 10^3 UV photons are created by a 50 keV electron. The prompt photon signal and a delayed signal from quantum evaporation initiated by the phonons/rotons at the free surface are detected by arrays of silicon or sapphire wafer calorimeters placed above the surface of the liquid. Position resolution is obtained from the distribution of the hit wafers and the timing difference of the prompt and delayed part of the signal.

For a ten-ton detector (size about $5 \times 5 \times 5$ m^3), the event rate expected from the reference solar model is 18 events/day from the pp flux and 7 events/day from the ^{7}Be flux [106]. The main source of background is Compton electrons from residual radioactivity in the cryostat external to the liquid. Background reduction is achieved by imposing topological cuts.

The 'R&D' conducted by the HERON collaboration demonstrated the feasibility in principle of the new detection concept and gave promising results [4, 106]. A major challenge to be accommodated is the improvement of the wafer sensitivity for use in large volumes by a factor of $\approx$20; employing recent developments of magnetic cryogenic calorimeters or superconducting transition-edge thermometers might lead to a breakthrough for this item.

7. Conclusions

Massive neutrinos in conjunction with flavour mixing among leptons had already been discussed as an attractive explanation of the solar neutrino puzzle many years ago. Recent years, however, with the availability of increasingly accurate measurements from several complementary experiments, have led to a qualitatively new situation in solar neutrino physics. As discussed in this article, from these results, evidence for massive neutrinos and therefore physics beyond the standard model can be concluded.

However, this evidence is still indirect, as it is exclusively based on the disappearance of electron neutrinos emitted from the Sun. With solar neutrinos, no straightforward appearance experiment is possible for energetic reasons. What remains, however, is the possibility of utilizing for detection of solar neutrinos both neutral-current and charged-current interactions. Following both avenues allows one to extract the flavour content. Obviously, this strategy constitutes a fully viable realization of the 'appearance' method.

As oscillation effects are generally energy dependent, the ultimate experimental challenge is the full spectroscopy of the solar neutrino spectrum via both neutral- and charged-current interactions. With the upcoming and near-future experiments, we will have the possibility of scrutinizing intrinsic neutrino parameters, i.e. masses and mixing angles, by determining separately the content of ν_e and $\nu_\mu + \nu_\tau$ for every individual neutrino branch emitted by our Sun.

Acknowledgments

It is a pleasure to thank T Hagner, W Hampel, M Junker, R E Lanou, Y Suzuki and many other colleagues for kindly providing us with material and information on the current status and future planning of their experiments and projects. MA particularly acknowledges stimulating discussions with G Raffelt and N Schmitz.

References

[1] Abdurashitov J N *et al* (SAGE Collaboration) 1996 *Phys. Rev. Lett.* **77** 4708
[2] Abdurashitov J N *et al* (SAGE Collaboration) 1999 *Phys. Rev.* C **59** 2246
(Abdurashitov J N *et al* (SAGE Collaboration) 1998 *Preprint* hep-ph/9803418)
[3] Abdurashitov J N *et al* (SAGE Collaboration) 1991 *Phys. Rev.* C **60** 055801
(Abdurashitov J N *et al* (SAGE Collaboration) 1999 *Preprint* astro-ph/9907113)
[4] Adams J S *et al* 1999 *Proc. Int. Workshop on Next Generation Detectors for Neutrinos and Nuclear Decay (Stony Brook, NY)*
[5] Adelberger E G *et al* 1998 *Rev. Mod. Phys.* **70** 1265
[6] Altmann M *et al* 1996 *Nucl. Instrum. Methods* A **381** 398
[7] Altmann M 1998 *Proc. NATO ASI on Masses of Fundamental Particles (Cargese, France, 5–17 August 1996)* ed M Levy *et al* (New York: Plenum) pp 205–14
[8] Altmann M, Hillebrandt W, Janka H-T and Raffelt G (ed) 1998 *Neutrino Astrophysics; Proc. 4th SFB-375 Ringberg Workshop (20–24 October 1997)* (Technische Universität München, Munich, Germany)
(Altmann M, Hillebrandt W, Janka H-T and Raffelt G 1998 *Preprint* astro-ph/9801320)
[9] Altmann M *et al* 1997 *Proc. 4th Int. Solar Neutrino Conf. (Heidelberg, Germany, 8–11 April)* ed W Hampel (ISBN 3-00-002064-0) pp 183–91
[10] Altmann M *et al* 1999 *Nucl. Phys.* B (Proc. Suppl.) **70** 374
[11] Angulo C *et al* (NACRE) 1999 *Nucl. Phys.* A **656** 3
[12] Assamagan K *et al* 1996 *Phys. Rev.* D **53** 6065
[13] Assenbaum H J *et al* 1987 *Z. Phys.* A **327** 461
[14] Athanassopoulos C *et al* 1996 *Phys. Rev. Lett.* **77** 3082
[15] Bahcall J N 1989 *Neutrino Astrophysics* (Cambridge: Cambridge University Press)
[16] Bahcall J N and Pinsonneault M 1992 *Rev. Mod. Phys.* **64** 885
[17] Bahcall J N *et al* 1997 *Phys. Rev. Lett.* **78** 171
[18] Bahcall J N 1997 *Phys. Rev.* C **56** 3391
[19] Bahcall J N, Basu S and Pinsonneault M H 1998 *Phys. Lett.* B **433** 1
(Bahcall J N, Basu S and Pinsonneault M H 1998 *Preprint* astro-ph/9805135)
[20] Bahcall J N *et al* 1998 *Phys. Rev.* D **58** 9601
[21] Bahcall J N *et al* 2000 *Phys. Lett.* B **477** 401
[22] Bahcall J N *Internet Homepage* http://www.sns.ias.edu/∼jnb
[23] Bandler S R *et al* 1995 *Phys. Rev. Lett.* **74** 3169
[24] Bang J *et al* 1996 *Phys. Rev.* C **53** R18
[25] Basu S and Antia H M 1995 *Mon. Not. R. Astron. Soc.* **276** 1402
[26] Basu S and Antia H M 1997 *Mon. Not. R. Astron. Soc.* **287** 189
[27] Berezinsky V *et al* 1994 *Phys. Lett.* B **341** 38
[28] Berezinsky V *et al* 1999 *Phys. Rev.* D **60** 123 002
[29] Bonetti R *et al* (LUNA Collaboration) 1999 *Phys. Rev. Lett.* **82** 5205
[30] Brun A S, Turck-Chièze S and Morel P 1998 *Astrophys. J.* **506** 913
(Brun A S, Turck-Chièze S and Morel P 1998 *Preprint* astro-ph/9806272)
[31] BOREXINO Collaboration 2001 *Astropart. Phys.* to be submitted
[32] Carter J R 1992 *Proc. Joint Int. Lepton–Photon Symp. and Europhys. Conf. on High Energy Physics (Geneva, Switzerland, 1991)* ed S Hegarthy *et al* (Singapore: World Scientific)
[33] Caso C *et al* (Particle Data Group) 1998 *Euro. Phys. J.* C **3** 1
[34] Castellani V *et al* 1994 *Phys. Rev.* D **50** 4749
[35] Castellani V *et al* 1997 *Phys. Rep.* **281** 309
[36] Chadwick J 1932 *Proc. R. Soc.* A **136** 692
[37] Christensen-Dalsgaard J *et al* 1996 *Science* **272** 1286
[38] Cleveland B 1983 *Nucl. Instrum. Methods* A **214** 451
[39] Cleveland B *et al* 1997 *Proc. 4th Int. Solar Neutrino Conf. (Heidelberg, Germany, 8–11 April)* ed W Hampel (ISBN 3-00-002064-0) p 85
[40] Cleveland B *et al* 1997 *Proc. 4th Int. Solar Neutrino Conf. (Heidelberg, Germany, 8–11 April)* ed W Hampel (ISBN 3-00-002064-0) p 228
[41] Cowan C L *et al* 1956 *Science* **124** 103
[42] Cribier M *et al* 1996 *Nucl. Instrum. Methods* A **378** 233
[43] Cribier M 1998 *Low Energy Neutrino Spectroscopy, Mtg (Assergi, Italy, 28 July)*
[44] Cummings A and Haxton W 1996 *Phys. Rev. Lett.* **77** 4286

[45] BOREXINO Collaboration 1998 *Astropart. Phys.* **8** 141
[46] BOREXINO Collaboration 1998 *Phys. Lett.* B **422** 349
[47] Danby G *et al* 1962 *Phys. Rev. Lett.* **9** 36
[48] Davis R *et al* 1968 *Phys. Rev. Lett.* **20** 1205
[49] Davis R *et al* 1997 *Proc. 4th Int. Solar Neutrino Conf. (Heidelberg, Germany, 8–11 April)* ed W Hampel (ISBN 3-00-002064-0) p 64
[50] McDonald A B (SNO Collaboration) 1999 *Nucl. Phys.* B (Proc. Suppl.) **77** 43
[51] Eddington A S 1920 *Observatory* **43** 341
[52] Engel J *et al* 1991 *Phys. Rev. Lett.* **67** 426
[53] Engel J *et al* 1994 *Phys. Rev.* C **50** 1702
[54] Ewan G 1992 *Nucl. Instrum. Methods* A **314** 373
[55] Fogli G L *et al* 2000 *Phys. Rev.* D 61 073 009
[56] Fukuda Y (SUPERKAMIOKANDE Collaboration) 1999 *Phys. Rev. Lett.* **82** 2430
[57] Galeazzi M *et al* 1997 *Phys. Lett.* B **398** 187
[58] GALLEX Collaboration (Anselmann P *et al*) 1992 *Phys. Lett.* B **285** 376
[59] GALLEX Collaboration (Anselmann P *et al*) 1992 *Phys. Lett.* B **285** 390
[60] GALLEX Collaboration (Anselmann P *et al*) 1993 *Phys. Lett.* B **314** 445
[61] GALLEX Collaboration (Anselmann P *et al*) 1994 *Phys. Lett.* B **327** 377
[62] GALLEX Collaboration (Anselmann P *et al*) 1995 *Phys. Lett.* B **342** 440
[63] GALLEX Collaboration (Anselmann P *et al*) 1995 *Phys. Lett.* B **357** 237
[64] GALLEX Collaboration (Hampel W *et al*) 1996 *Phys. Lett.* B **388** 384
[65] GALLEX Collaboration (Hampel W *et al*) 1998 *Phys. Lett.* B **420** 114
[66] GALLEX Collaboration (Hampel W *et al*) 1998 *Phys. Lett.* B **436** 158
[67] GALLEX Collaboration (Hampel W *et al*) 1999 *Phys. Lett.* B **447** 127
[68] GALLEX Collaboration 2001 The GALLEX solar neutrino experiment *Astropart. Phys.* to be submitted
[69] Gamow G 1928 *Z. Phys.* **52** 510
[70] Gavrin V (SAGE Collaboration) 2000 *Neutrino-2000: 19th Int. Conf. on Neutrino Physics and Astrophysics (Sudbury, Canada, June)* talk
[71] GNO Collaboration 1996 *Proposal for a Permanent Gallium Neutrino Observatory at Gran Sasso, Milano* reprinted in *LNGS Annual Report 1996* Laboratori Nazionali del Gran Sasso, Italy (available from http://www.mpi-hd.mpg.de/∼kirsten/)
[72] Bellotti E (GNO Collaboration) 2001 *Neutrino-2000: 19th Int. Conf. on Neutrino Physics and Astrophysics (Sudbury, Canada, June 2000); Nucl. Phys.* B (Proc. Suppl.) at press
[73] GNO Collaboration (Altmann M *et al*) 2000 *Phys. Lett.* B **490** 16
(GNO Collaboration (Altmann M *et al*) 2000 *Preprint* hep-ex/0006034)
[74] Goldhaber M *et al* 1958 *Phys. Rev.* **109** 1015
[75] Gough D O *et al* 1996 *Science* **272** 1281
[76] Gough D O *et al* 1996 *Science* **272** 1297
[77] Graboske H C *et al* 1973 *Ap. J.* **181** 457
[78] Grevesse N and Noels A 1993 *Origin and Evolution of the Elements* ed N Pratzos *et al* (Cambridge: Cambridge University Press) p 15
[79] Gribov V and Pontecorvo B 1969 *Phys. Lett.* B **28** 463
[80] Gruzinov A V and Bahcall J N 1997 *Ap. J.* **490** 437
[81] Gruzinov A V and Bahcall J N 1998 *Ap. J.* **504** 996
[82] Hagner T *et al* 2000 *Astropart. Phys.* **14** 33
[83] Hampel W and Remsberg L 1985 *Phys. Rev.* C **31** 677
[84] Hampel W (ed) 1997 *Proc. 4th Int. Solar Neutrino Conf. (Heidelberg, Germany, 8–11 April)* (ISBN 3-00-002064-0)
[85] Harvey J W *et al* 1996 *Science* **272** 1285
[86] Hata N and Haxton W C 1995 *Phys. Lett.* B **353** 422
[87] Haxton W C 1988 *Phys. Rev. Lett.* **60** 768
[88] Haxton W C 1998 *Phys. Lett.* B **431** 110
[89] von Hentig R 1998 *Proc. Int. Conf. on Advanced Technology and Particle Physics (Como, Italy, 5–9 October)*
[90] Heusser G 1993 *Trends in Astroparticle Physics* ed P C Bosetti (Stuttgart: Teubner) p 33
[91] Hirata K S *et al* 1990 *Phys. Rev. Lett.* **65** 1301
[92] Johnson C W *et al* 1992 *Ap. J.* **392** 320
[93] Junker M 1996 *Doctoral Dissertation* Universität Bochum, Germany
[94] Junker M *et al* (LUNA Collaboration) 1998 *Phys. Rev.* C **57** 2700

[95] Junker M 1999 personal communication
[96] KAMIOKANDE Collaboration 1996 *Phys. Rev. Lett.* **77** 1683
[97] Kirsten T A 1999 *Rev. Mod. Phys.* **71** 1213
[98] Kopylov A *et al* 1997 *Proc. 4th Int. Solar Neutrino Conf. (Heidelberg, Germany, 8–11 April)* ed W Hampel (ISBN 3-00-002064-0) p 263
[99] Kraus L and Wilczek F 1985 *Phys. Rev. Lett.* **55** 122
[100] Kuzmin V A 1966 *Sov. Phys.–JETP* **22** 1050
[101] Iglesias C A and Rogers F J 1996 *Astrophys. J.* **464** 943
[102] Lachenmaier T 2000 *Diploma Thesis* Technische Universität München, Munich, Germany
[103] Langacker P 1983 *Phys. Rev.* D **27** 1228
[104] Langanke K *et al* 1996 *Phys. Lett.* B **369** 211
[105] Lande K *et al* 1999 *Nucl. Phys.* B (Proc. Suppl.) **77** 13
[106] Lanou R E 1999 *Nucl. Phys.* B (Proc. Suppl.) **77** 55
[107] LENS Collaboration 1999 *Letter of Intent* addressed to the Scientific Committee of Laboratori Nazionali del Gran Sasso, Italy, January 1999
[108] Loeb A 1989 *Phys. Rev.* D **39** 1009
[109] LUNA Collaboration 1996 *Phys. Lett.* B **389** 452
[110] Maki Z *et al* 1962 *Prog. Theor. Phys.* **28** 870
[111] Mikheyev S and Smirnov A 1985 *Sov. J. Nucl. Phys.* **42** 913
Mikheyev S and Smirnov A 1986 *Nuovo Cimento* **9** C 17
[112] Motobayashi T *et al* 1994 *Phys. Rev. Lett.* **73** 2680
[113] Nussinov S 1976 *Phys. Lett.* B **63** 201
[114] Pauli W 1930 *Letter* reprinted in 1990 *Neutrino Physics* ed K Winter (Cambridge: Cambridge University Press)
[115] Pontecorvo B 1958 *Sov. Phys.–JETP* **6** 429
Pontecorvo B 1958 *Sov. Phys.–JETP* **7** 172
[116] Pontecorvo B 1967 *Zh. Eksp. Teor. Fiz.* **53** 1717
[117] Pontecorvo B 1968 *Sov. Phys.–JETP* **26** 984
[118] Raghavan R S 1997 *Phys. Rev. Lett.* **78** 3618
[119] Raghavan R S *et al* 1998 *Phys. Rev. Lett.* **80** 635
[120] Raghavan R S 1998 *Proc. Int. Workshop on Low Energy Neutrino Spectroscopy, LENS (Assergi, Italy, 28 July)*
[121] Reines F and Cowan C L 1956 *Nature* **178** 446
[122] Rodeback G W and Allen G S 1952 *Phys. Rev.* **86** 446
[123] Rogers F J *et al* 1996 *Astrophys. J.* **456** 902
[124] Rolfs C E and Rodney W 1988 *Cauldrons in the Cosmos* (Chicago, IL: University of Chicago Press)
[125] Salpeter E E 1954 *Aust. J. Phys.* **7** 373
[126] Schanda U and Urban A 1996 *Nucl. Instrum. Methods* A **381** 79
[127] Schlattl H and Weiss A 1998 *Neutrino Astrophysics; Proc. 4th SFB-375 Ringberg Workshop (20–24 October 1997)* ed M Altmann, W Hillebrandt, H-T Janka and G Raffelt (Technische Universität München, Munich, Germany) p 19
[128] Schlattl H *et al* 1997 *Astron. Astrophys.* **322** 646
[129] Schönert S 1999 *Nucl. Phys.* B (Proc. Suppl.) **70** 195
[130] McDonald A (SNO Collaboration) 2001 *19th Int. Conf. on Neutrino Physics and Astrophysics (Sudbury, Canada, June 2000); Nucl. Phys.* B (Proc. Suppl.) at press
[131] Stix M 1998 *Neutrino Astrophysics; Proc. 4th SFB-375 Ringberg Workshop (20–24 October 1997)* ed M Altmann, W Hillebrandt, H-T Janka and G Raffelt (Technische Universität München, Munich, Germany) p 13
[132] Stodolsky L 1998 *Phys. Rev.* D **58** 36 006
[133] Suzuki Y (SUPERKAMIOKANDE Collaboration) 1999 *Nucl. Phys.* B (Proc. Suppl.) **77** 35
[134] Suzuki A (KAMLAND Collaboration) 1999 *Nucl. Phys.* B (Proc. Suppl.) **77** 171
[135] Suzuki Y (SUPERKAMIOKANDE Collaboration) 2001 *19th Int. Conf. on Neutrino Physics and Astrophysics, (Sudbury, Canada, June 2000); Nucl. Phys.* B (Proc. Suppl.) at press
[136] Takcuchi Y (SUPERKAMIOKANDE Collaboration) 1999 *Phys. Lett.* B **452** 418
[137] Turck-Chièze S *et al* 1993 *Phys. Rep.* **230** 57
[138] Turck-Chièze S and Lopes I 1993 *Ap. J.* **408** 347
[139] Turck-Chièze S and Brun S 1997 *Proc. 4th Int. Solar Neutrino Conf. (Heidelberg, Germany, 8–11 April)* ed W Hampel (ISBN 3-00-002064-0) p 41
[140] Turck-Chièze S 2001 *19th Int. Conf. on Neutrino Physics and Astrophysics (Sudbury, Canada, June 2000); Nucl. Phys.* B (Proc. Suppl.) at press

[141] Urban A 1989 *Doctoral Dissertation* Technische Universität München, Munich, Germany
[142] Wänninger S *et al* 1999 *Phys. Rev. Lett.* **83** 1088
[143] Wänninger S 2000 *Doctoral Dissertation* Technische Universität München, Munich, Germany
[144] Weinheimer C (Mainz Collaboration) 2001 *19th Int. Conf. on Neutrino Physics and Astrophysics (Sudbury, Canada, June 2000); Nucl. Phys.* B (Proc. Suppl.) at press
[145] Winter K (ed) 1990 *Neutrino Physics* (Cambridge: Cambridge University Press)
[146] Wink R *et al* 1993 *Nucl. Instrum. Methods* A **329** 541
[147] Wolfenstein L 1978 *Phys. Rev.* D **17** 2369
[148] Wolfenstein L 1979 *Phys. Rev.* D **20** 2634
[149] Glashow S L, Iliopoulos J and Maiani L 1970 *Phys. Rev.* D **2** 1285